Tectonophysics 488 (2010) 87–109

Contents lists available at ScienceDirect

Tectonophysics

journal homepage: www.elsevier.com/locate/tecto

Neogene structural evolution of the Sierra San Felipe, Baja California: Evidence for proto-gulf transtension in the Gulf Extensional Province?

Christian Seiler [a,*], John M. Fletcher [b], Mark C. Quigley [c], Andrew J.W. Gleadow [a], Barry P. Kohn [a]

[a] School of Earth Sciences, The University of Melbourne, Victoria 3010, Australia
[b] Departamento de Geología, CICESE, Km 107 Carr. Tijuana–Ensenada, Ensenada, BC 22800, Mexico
[c] Department of Geological Sciences, University of Canterbury, Christchurch 8140, New Zealand

ARTICLE INFO

Article history:
Received 26 June 2008
Received in revised form 29 July 2009
Accepted 28 September 2009
Available online 7 October 2009

Keywords:
Extensional tectonics
Transtension
Paleostress
Proto-gulf
Gulf Extensional Province
Baja California

ABSTRACT

The Sierra San Felipe, located in the Gulf Extensional Province of northeastern Baja California, experienced a complex deformation history of integrated normal and strike-slip faulting, block rotations and extension-parallel folding as a result of Neogene transtensional plate margin shear between the Pacific and North American plates. The eastern range-front of the Sierra San Felipe is defined by three left-stepping, en-echelon detachment faults that are linked by dextral and sinistral transfer faults and accommodation zones. The Las Cuevitas, Santa Rosa and Huatamote detachments comprise NE- to SE-dipping, moderate- to low-angle normal faults that accommodate between ~1.5 and 9 km of broadly E- to SE-directed extension and show strong along-strike displacement gradients. Hanging wall half-grabens are infilled with northwest tilted Miocene–Pliocene volcanic and sedimentary rocks that have been deposited nonconformably onto the batholithic basement. Stratigraphic relationships indicate that faulting on the Las Cuevitas and Santa Rosa detachment faults initiated synchronously as a kinematically linked fault system before ~7 Ma (~9–8 Ma based on the timing of footwall exhumation), during the so-called 'proto-gulf' phase of rifting. Paleostress calculations suggest a transtensional stress regime with NE- to SE-directed extension and permutating vertical to N–S trending, subhorizontal contraction. Fault kinematics and paleostress orientations of the fault array do not vary through time, but reflect the spatial distribution of fault planes with respect to a transtensional stress regime that lasted throughout the entire slip history of the detachments. Our data indicate that clockwise vertical-axis block rotations and constrictional folding were an integral part of the deformation history in the Sierra San Felipe since rifting began in the late Miocene, and may have played an important role in facilitating the transfer of deformation between the Main Gulf Escarpment and offshore faults in the Gulf of California. These observations support the hypothesis that middle Miocene to present oblique-divergent plate motion was accommodated by a single phase of integrated transtensional shearing in the Gulf Extensional Province.

1. Introduction

As a rare example of a youthful oceanic basin, the Gulf of California presents unique insights into the transition from continental rifting to oceanic spreading and the formation of passive margins. Neogene opening of the Gulf of California initiated in response to a major plate boundary reorganisation that followed the demise of the subduction zone along the western margin of Baja California. Incipient interaction between the Pacific and North American plates induced deformation in the continental borderland west of Baja California as well as in the Gulf Extensional Province, a region of highly extended continental crust surrounding and encompassing the Gulf of California (e.g. Karig and Jensky, 1972; Spencer and Normark, 1979; Hausback, 1984; Lonsdale, 1989; Stock and Hodges, 1989; Lonsdale, 1991; Fletcher et al., 2007).

Present-day relative plate motion between the Pacific and North American plates is largely accommodated by the en-echelon array of right-stepping transform faults and nascent oceanic spreading centres in the Gulf of California (Fig. 1). Plate motion models coupled with geodetic observations suggest that the transfer of the Baja California microplate from the North American to the Pacific plate was a gradual process, beginning at ~12 Ma (Stock and Hodges, 1989) and continuing until at least ~1 Ma ago (DeMets, 1995; DeMets and Dixon, 1999), although transfer may still be ongoing (Dixon et al., 2000; Fletcher and Mungúia, 2000; Michaud et al., 2004).

The capture of the Baja California microplate traditionally has been thought to have occurred in two distinct kinematic phases (e.g. Hausback, 1984; Stock and Hodges, 1989): (1) an early (~12–6 Ma) proto-gulf phase when plate margin shearing was kinematically

* Corresponding author.
E-mail addresses: seilerc@unimelb.edu.au (C. Seiler), jfletche@cicese.mx (J.M. Fletcher), mark.quigley@canterbury.ac.nz (M.C. Quigley), gleadow@unimelb.edu.au (A.J.W. Gleadow), b.kohn@unimelb.edu.au (B.P. Kohn).

0040-1951/$ – see front matter © 2009 Elsevier B.V. All rights reserved.
doi:10.1016/j.tecto.2009.09.026

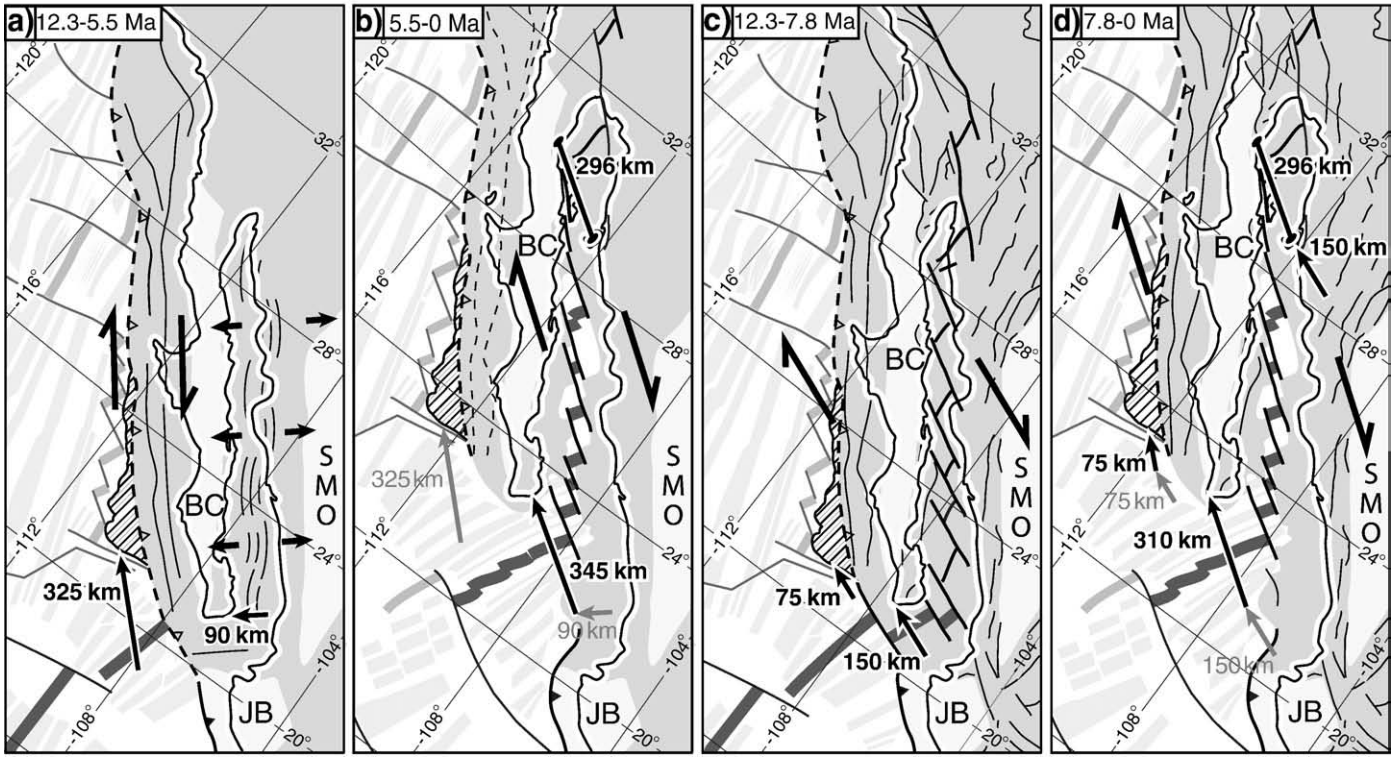

Fig. 1. Existing kinematic models for the plate tectonic evolution of the Gulf of California (modified from Fletcher et al., 2007). *Two-stage model:* (a) Kinematic partitioning between strike-slip faulting west of Baja California accommodating ~325 km of slip, and ~90 km orthogonal, ENE-directed rifting in the Gulf Extensional Province between 12.3 and 5.5 Ma. (b) Deformation on transfer faults west of Baja started waning at ~5.5 Ma, when the Pacific–North America plate motion re-localised into the axis of the modern Gulf of California, producing ~345 km of transtensional deformation. *Single-stage model:* (c) Transtensional shear affected two spatially separated deformation belts on opposite sides of Baja California between 12.3 and 7.8 Ma and produced approximately 75 km and 150 km offset in the continental borderland and the Gulf Extensional Province, respectively. (d) Following a clockwise rotation of the relative plate motion at ~7.8 Ma, integrated oblique-divergent slip continued in both deformation belts to the present and accumulated a further 75 km and 310 km of displacement west of Baja and in the Gulf Extensional Province, respectively. Continental crust affected by Neogene deformation is shown in medium grey, unfaulted blocks in light grey, and magnetic anomalies in faint grey. Active oceanic spreading centres are shown as thick grey lines, abandoned rift segments as light grey lines; inactive faults are dashed. Position of the Magdalena fan (piercing point used by Fletcher et al., 2007) shown in striped pattern. Black line with handles in (b) and (d) connects volcanic deposits correlated by Oskin and Stock (2003b). BC = Baja California microplate, JB = Jalisco block, and SMO = Sierra Madre Occidental.

partitioned into transform faulting west of Baja California and orthogonal rifting in a NE–SW direction in the Gulf Extensional Province (Fig. 1a); and (2) a later phase (~6 Ma to present) of integrated transtensional shearing within the Gulf of California (Fig. 1b). Although no dynamic explanation has been proposed for this kinematic model, an early period of orthogonal rifting most likely would have been related to gravitational collapse of over-thickened crust in the Gulf Extensional Province.

The long-held view of a two-stage tectonic evolution of the Gulf of California has recently been challenged in light of new geophysical and geochronological data. Fletcher et al. (2007) documented the existence of a major normal fault named the Santa Margarita–San Lazaro fault that extends 400–500 km along the length of the continental shelf west of Baja California, which demonstrates the transtensional nature of Neogene shearing in this deformation belt. Using regional piercing points, they further demonstrated that the magnitude of dextral strike-slip displacement west of Baja California is significantly less than previously assumed, which requires additional strike-slip motion in the Gulf Extensional Province in order to satisfy the finite displacement estimates of global plate-circuit motion models. Therefore, Fletcher et al. (2007) proposed an alternative kinematic model (Fig. 1c, d) of integrated transtensional deformation on both sides of the Baja California microplate since the onset of shearing between the Pacific and North American plates in the middle Miocene. In this model, the distribution and kinematics of shearing is more strongly controlled by lithospheric weaknesses than possible gravitational instabilities in the continental crust of the Gulf Extensional Province (Fletcher et al., 2007).

The two models differ primarily in the proposed kinematics of faulting during the early stages of Neogene extension (Fig. 1a, c). Numerous structural studies in Baja California have documented multiple phases of faulting with distinct kinematics in the Gulf Extensional Province that were interpreted to represent a clockwise rotation of the extension direction as the Gulf Extensional Province supposedly changed from NE-directed proto-gulf rifting to the modern transtensional stress regime (e.g. Angelier et al., 1981; Zanchi, 1994; Umhoefer et al., 2002). In fact, fault-slip data still provide the only direct observational data that is compatible with the two-phase rifting model.

In this study, we present a detailed structural and kinematic analysis of a complex fault network on the rifted margin of Baja California. The Sierra San Felipe, located in the northern Gulf Extensional Province (Figs. 2 and 3), contains key structural relationships to characterise the kinematics of rifting along the margin of Baja California. Virtually every major class of faults is exposed in a complex array that cuts rocks ranging in age from Cretaceous to early Pleistocene, which provides a unique opportunity to evaluate spatial and temporal variations in fault kinematics across the rifted margin of Baja California. Our data demonstrate multiple directions of extension that are tempting to interpret according to a multi-phase tectonic model. However, we argue that the data fit equally well or better with a kinematic model of progressive transtensional shearing, which involves highly three-dimensional strain and a combination of vertical- and horizontal-axis block rotations.

2. Regional tectonic setting

2.1. Main Gulf Escarpment

The Main Gulf Escarpment has been described as the break-away fault of continental rifting in the Gulf Extensional Province (Gastil et al., 1975). At the latitude of the Sierra San Felipe, the escarpment is defined by the east-dipping Sierra San Pedro Mártir fault, which produces a 1000–2500 m high topographic escarpment that extends ~100 km along strike (Figs. 2 and 3). The San Pedro Mártir fault accommodates ~5 km of vertical offset across its central segments (Hamilton, 1971; Gastil et al., 1975) and slip decreases systematically to the north and south, where no more than 800 m of offset is

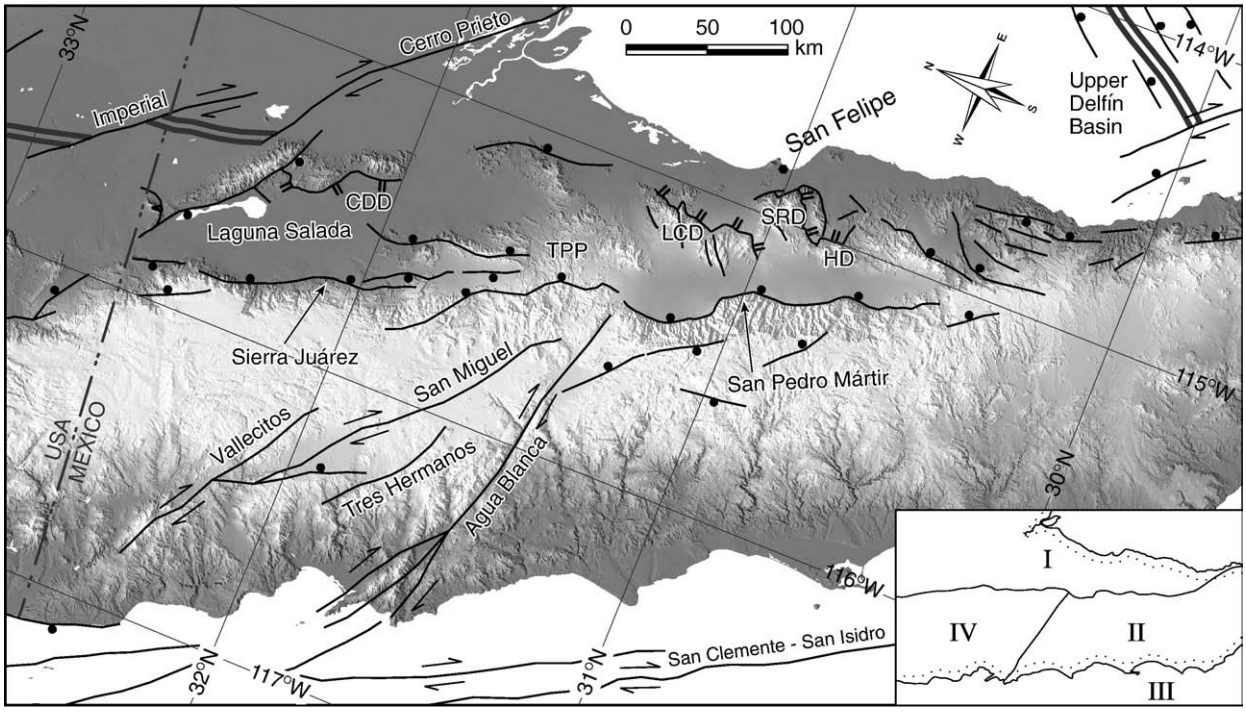

Fig. 2. Digital elevation model with tectonic setting of northern Baja California showing main active or recently active faults (after Gastil et al., 1975; Fenby and Gastil, 1991; Ness and Lyle, 1991; Axen and Fletcher, 1998; this study). Inset shows the four major structural provinces of Baja California: I) the Gulf Extensional Province along eastern Baja, II) the relatively unextended central and western portion of the peninsula, III) the sheared continental borderland west of Baja California, and IV) the transpeninsular strike-slip province north of the Agua Blanca fault. CDD = Cañada David detachment, HD = Huatamote detachment, LCD = Las Cuevitas detachment, SRD = Santa Rosa detachment, and TPP = Sierra Tinaja–Sierra Pinta volcanic province.

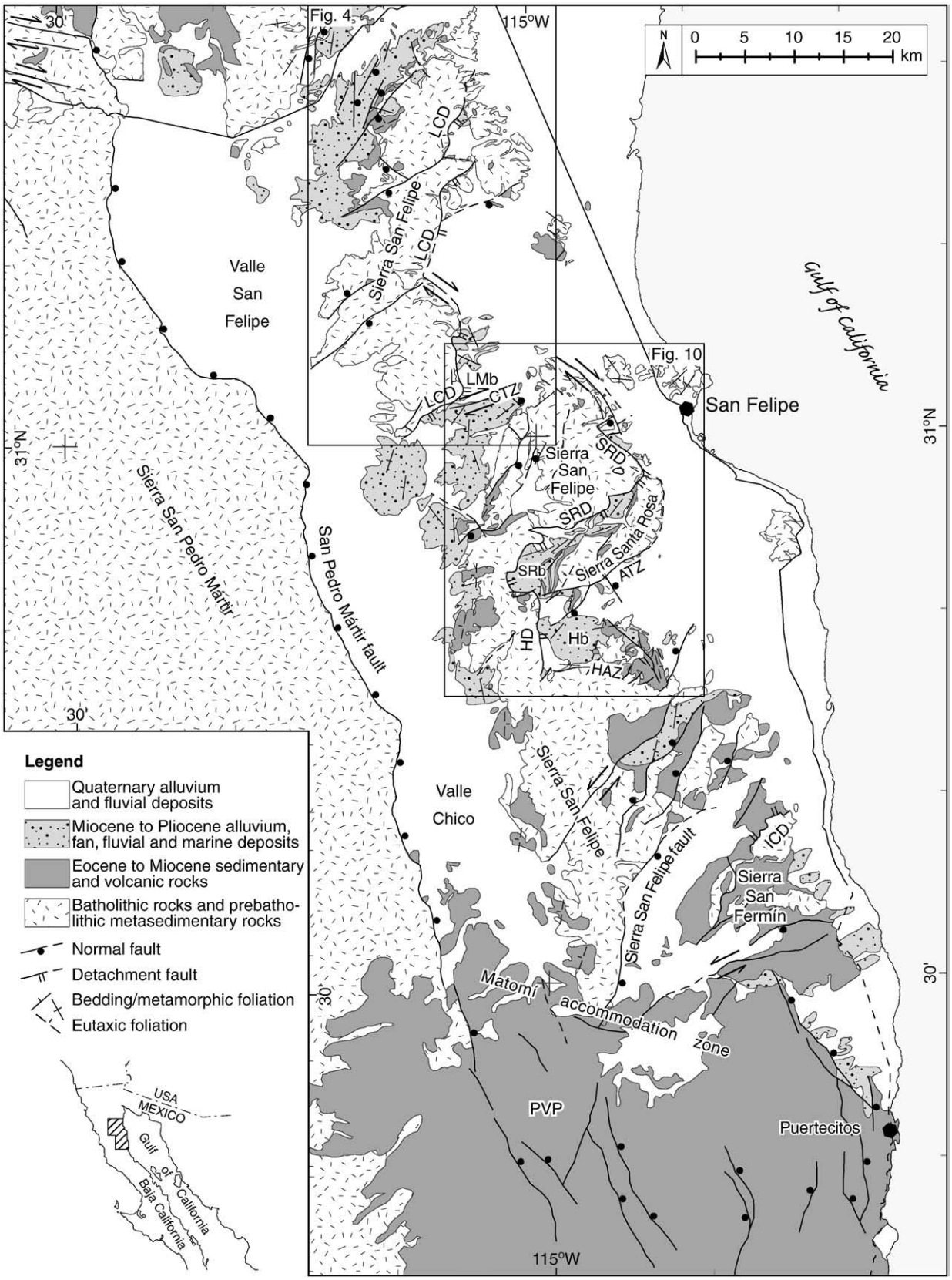

Fig. 3. Regional geological map of the Gulf Extensional Province in northeastern Baja California showing the basin and range topography of the Sierras San Felipe and Santa Rosa (simplified from Andersen, 1973; Gastil et al., 1975; Lewis and Stock, 1998a; Stock, 2000; Oskin, 2002; Black, 2004; this study). The en-echelon, left-stepping geometry of the highly curviplanar Las Cuevitas, Santa Rosa and Huatamote detachments represents the next dominant set of normal faults from the break-away fault, the San Pedro Mártir fault, in direction of movement. Boxes indicate the locations of Figs. 4 and 10. ATZ = Amarillas transfer zone, CTZ = Cuevitas transfer zone, HAZ = Huatamote accommodation zone, Hb = Huatamote basin, HD = Huatamote detachment, ICD = Ironwood Canyon detachment, LCD = Las Cuevitas detachment, LMb = Llano El Moreno basin, PVP = Puertecitos volcanic province, SRb = Santa Rosa basin, and SRD = Santa Rosa detachment.

accumulated (Stock and Hodges, 1990). The scalloped trace of the San Pedro Mártir fault and the strong tilting of pre-extensional strata in its hanging wall compared to the footwall strata suggest it has a listric geometry at depth (Hamilton, 1971; Dokka and Merriam, 1982). Scarps up to 25 m cut late Quaternary alluvial fans, and modern activity on the Sierra San Pedro Mártir fault was demonstrated by a magnitude (M_L) 5.5 earthquake in 1974 (Brown, 1978).

2.2. Transpeninsular strike-slip province

The transpeninsular strike-slip province comprises two major strike-slip faults that transect the peninsula in northern Baja California (Fig. 2). The WNW-striking Agua Blanca fault accommodated between ~11 and 23 km of finite right-lateral slip, with ~5 km of displacement recorded by Quaternary(?) fan deposits (Allen et al., 1960). Neogene dextral movement is believed to have been superimposed on a late Mesozoic period of sinistral transpression on the ancestral Agua Blanca fault (Wetmore et al., 2002, 2003). The NW-striking San Miguel–Vallecitos fault system exhibits no more than ~500–600 m of right-lateral displacement (Harvey, 1985), which may reflect the incipient nature of the fault system (Hirabayashi et al., 1996). Both the Agua Blanca and San Miguel–Vallecitos faults are currently active and accumulate strain with a combined slip rate of ~4–8 mm/yr (Dixon et al., 2002).

The mechanism of displacement transfer between the transpeninsular strike-slip province and the Gulf Extensional Province is complex, as both fault systems die out eastward and neither fault can be traced across the Main Gulf Escarpment (Fig. 3; Allen et al., 1960; Hilinski, 1988). Instead, right-lateral shear appears to be distributed across multiple smaller-scale strike-slip and oblique-slip faults, which may play an important role in the transfer of strain between the Gulf Extensional Province and the transpeninsular strike-slip province (Lee et al., 1996).

2.3. Gulf Extensional Province

The Gulf Extensional Province exhibits a typical basin and range topography, where depositional basins such as the NNW trending Valle San Felipe–Valle Chico are bound by topographically elevated fault blocks like those that make up the Sierras San Felipe and Santa Rosa (Figs. 2 and 3). The Sierras San Felipe and Santa Rosa represent tilted extensional allochthons in the hanging wall of the San Pedro Mártir fault. Miocene to Pliocene volcanic and sedimentary strata along the western edge of the Sierra San Felipe are tilted westwards (Gastil et al., 1975; Dokka and Merriam, 1982; Stock, 1993; this study) and project below the Valle San Felipe–Valle Chico into the San Pedro Mártir fault (Fig. 3).

The northern and central Sierra San Felipe is bound to the east by three highly curviplanar low-angle normal fault systems, the Las Cuevitas, Santa Rosa and Huatamote detachments (Fig. 3), which juxtapose metamorphic and batholithic basement of the Sierra against Miocene to Pliocene sedimentary and volcanic rocks (Bryant, 1986; Black, 2004; this study). Transfer of deformation between the detachment faults is facilitated by both right- and left-lateral accommodation and transfer zone structures. Although no range-bounding fault crops out along the eastern margin of the Sierra Santa Rosa, the presence of a steep escarpment next to an extensive bajada suggests that this range-front is also controlled by a major fault (Fig. 3).

The southern Sierra San Felipe is bound to the east by the high-angle Sierra San Felipe normal fault, which exhibits moderate (>700 m; Stock and Hodges, 1990) normal displacement and possibly roots into the west-dipping Ironwood Canyon detachment of the Sierra San Fermín (Fig. 3; Lewis, 1994; Lewis and Stock, 1998a). No major fault has been reported on the eastern margin of the Sierra San Fermín, and its highly sinuous trace indicates that it is not controlled by a single fault.

At its southern end, the San Pedro Mártir fault steps east to the coast of the Gulf of California in the northern Puertecitos volcanic province, a Miocene to Pliocene ignimbrite field, defining an accommodation zone of closely spaced, small-displacement NNW-striking normal faults (Stock and Hodges, 1990; Nagy, 2000; Stock, 2000).

3. Lithological description of the Sierra San Felipe

3.1. Basement and pre-late Miocene strata

The basement of the Sierra San Felipe consists of Paleozoic to Mesozoic metamorphic rocks (Pbs) that have been intruded by large volumes of granodioritic to tonalitic batholiths (Kg) during the Cretaceous. Apatite fission track results document that post-emplacement cooling and final unroofing of the uppermost basement occurred at ~45–35 Ma (Seiler, 2009). Erosion produced a late Eocene(?) to Oligocene nonconformity above a gently undulating topography with roughly ENE–WSW oriented drainages (Dorsey and Burns, 1994). Due to its widespread occurrence and a subdued topographic expression, the basal unconformity is an excellent structural marker horizon to estimate fault displacements in the Sierra San Felipe, as has been demonstrated in adjacent areas (e.g. Axen and Fletcher, 1998).

A discontinuous veneer of interbedded fluvial sandstones and conglomerates (Tos) has been deposited onto the basal nonconformity. While sandstones are mostly locally derived, conglomerates contain both local and exotic clast assemblages. The basal sediments are typically less than 10 m thick, but attain a thickness of at least 400–450 m in a lacustrine depocentre in the southeastern Huatamote basin (Fig. 3). These oldest post-batholithic sediments correspond to group 1 strata of Stock (1993) and are described in detail by Oskin and Stock (2003a).

Overlying the basal sediments are several discontinuous olivine–pyroxene–plagioclase basalt flows (Tmb1) with a typical thickness of ~10–20 m. Significant thickness variations occur over short distances, which likely reflects both pre-existing topography and the lateral margins of individual flows. In the northern Sierra San Felipe, these basalts are locally underlain by hornblende-bearing andesite flows (Andersen, 1973). In the Santa Rosa basin (Fig. 3), basalt flows yield whole-rock $^{40}Ar/^{39}Ar$ cooling ages of ~21–19 Ma (Seiler, unpublished data), while equivalent deposits in the Llano El Moreno basin (Fig. 3) have been dated at 19.4±0.5 Ma ($^{40}Ar/^{39}Ar$ whole-rock age; Esser and McIntosh, 2003).

The rhyolitic Tuff of San Felipe (Tsf; Stock et al., 1999; Nagy et al., 1999; Oskin and Stock, 2003b) consists of a densely welded, pink to red-brown, crystal- and lithic-rich ignimbrite with a well-developed eutaxic foliation and overlies the Miocene basalts nonconformably. At its base, the ignimbrite typically contains a dark-brown to black, phenocryst-bearing vitrophyre (<1–1.5 m thick) overlain by a spherulitic welded tuff (~3–5 m thick) that grades into a densely welded section of several meters to a few tens of meters. In the southeastern Llano El Moreno basin (Fig. 4), a pink to purple, densely welded rhyolite tuff containing ~10% sanidine phenocrysts and rare lithics was described by Andersen (1973) and Black (2004), and is here correlated with the Tuff of San Felipe. The Tuff of San Felipe is continuous over long distances, but decreases in thickness from about 150–180 m in the southeastern Sierra San Felipe (Oskin and Stock, 2003b), to a few meters in the north-central Sierra San Felipe. Recent $^{40}Ar/^{39}Ar$ analysis of alkali feldspars yielded a ~12.6 Ma age for the Tuff of San Felipe (Stock et al., 1999).

3.2. Late Miocene to Pliocene rocks

3.2.1. Overview of the late Miocene to Pliocene stratigraphy

The Tuff of San Felipe is overlain by an extensive section of pre- to mostly syn-tectonic basin-fill sediments with minor intercalated

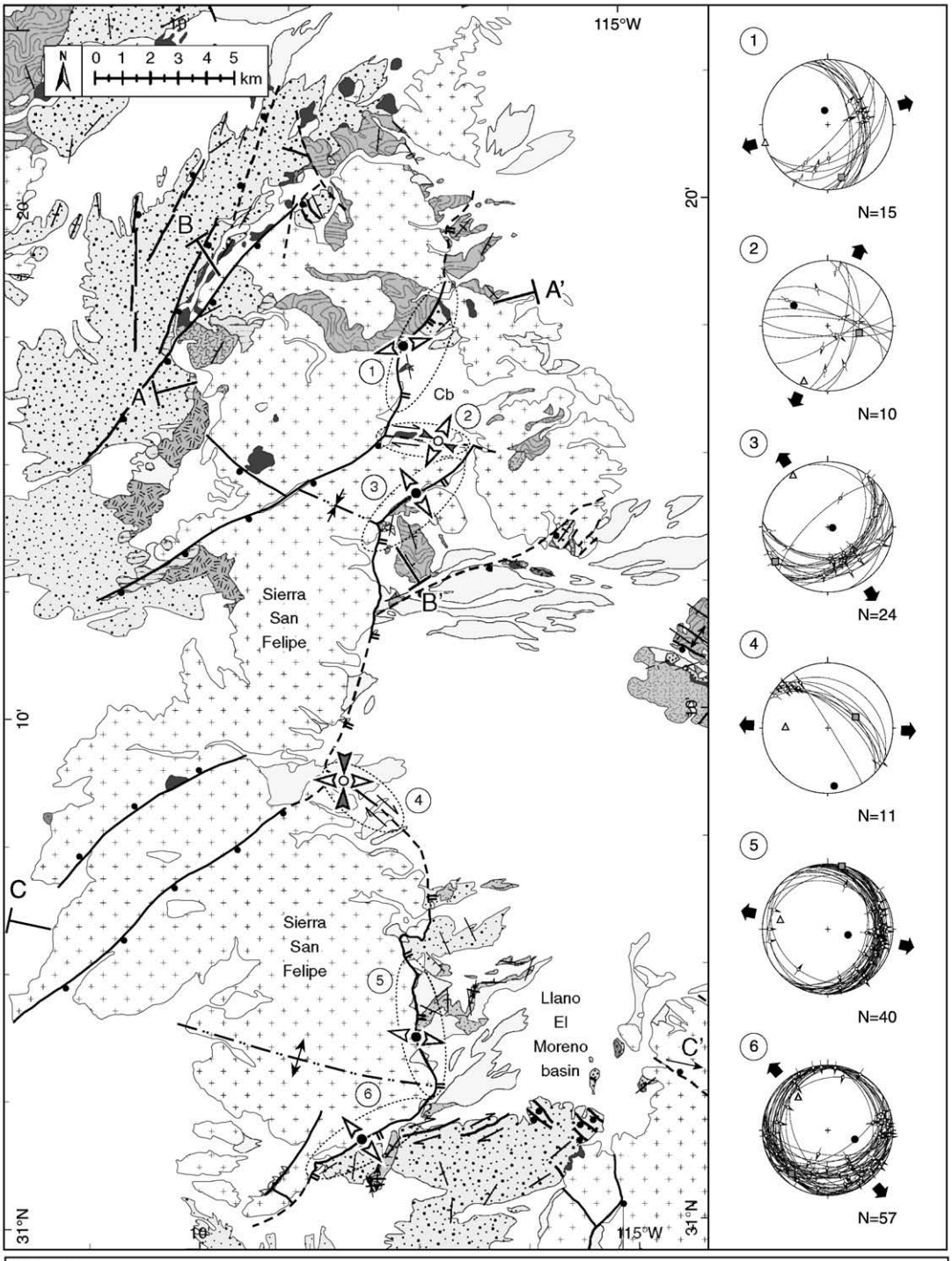

Legend

- Holocene alluvium and colluvium
- Older (Pleistocene?) alluvium, colluvium and fan deposits
- *angular unconformity*
- Tpm 2-6Ma — Late Miocene to Pliocene marine deposits, fossiliferous
- Tmf — Miocene to Pliocene alluvium, fan, fluvial and delta deposits, incl. fault scarp facies breccia
- Tma — Andesite lava flows with amphibole phenocrysts
- Dacite lava flows
- Tsf 12.6Ma — Densely welded, rhyolitic tuff (Tuff of San Felipe)
- Tmb1 19Ma — Olivine basalt
- Paleogene(?) Andesite lava flow with amphibole phenocrysts
- Tos — Basement derived fluvial deposits with exotic volcanic clasts
- *nonconformity*
- Kg — Cretaceous granodiorite to tonalite
- Pbs — Prebatholithic metasedimentary rocks
- Normal fault
- Detachment fault
- Bedding/met. foliation
- Eutaxic foliation
- Strike-slip kinematics
- Oblique-slip kinematics
- Dip-slip kinematics

volcanics that range in age from late Miocene to early Pleistocene. Syn-rift sediments dip predominantly to the W or NW into major basin-bounding normal faults and exhibit both lateral and vertical facies changes, which reflects a combination of proximal deposition from a tectonically induced topography as well as temporal variations in climate and tectonics of the basin. Deposition was largely synchronous with slip on the basin-bounding faults and as a result, the stratigraphic record of individual basins varies considerably.

The base of the late Miocene stratigraphy comprises discontinuously exposed, hornblende-bearing andesite flows (Tma) that have a thickness of up to ~100 m and where present, overlie the Tuff of San Felipe (Andersen, 1973; Bryant, 1986). The lowest syn-tectonic sediments (Tmf) typically comprise sandstones interbedded with pebble to boulder conglomerates. Clast composition of the conglomerate is highly reflective of adjacent lithologies, indicating a proximal origin for the fluvial deposits. Overall, basin-fill sediments fine upsection into crossbedded sandstones and sandstone–mudstone sequences with less abundant conglomerate channels, evaporite beds and dessication cracks, which indicates the development of a playa–lacustrine depocentre that we interpret to record the peak subsidence rate of the basins. These fine-grained syn-rift sediments coarsen upwards to a section of footwall derived fluvial conglomerate and clast-supported megabreccia containing angular clasts with partially striated or chloritised surfaces. The youngest strata are Pleistocene alluvial fan deposits that overlap the basin-bounding faults.

3.2.2. Llano El Moreno basin

The Llano El Moreno basin is a half-graben in the hanging wall of the Las Cuevitas detachment and contains late Miocene to Pliocene growth strata that overlie the pre-rift volcanics and basal sediments (Figs. 3 and 4). The southern portion of the basin contains the most complete exposure of the sequence, and pre-rift volcanics here dip more steeply (~10–40°) than overlying syn-rift sediments (~5–35°), which reflects syn-depositional tilting of the basin (Black, 2004). Overlying a lower section of alluvial strata are Miocene to Pliocene marine deposits (Tpm) that likely represent the development of a depocentre with maximum topographic subsidence in the basin. The oldest exposed marine unit is a finely laminated diatomite member containing late Miocene microfossils (~6.0–5.5 Ma; Boehm, 1984). This is overlain by a siltstone unit that contains diverse diatom and benthonic foraminiferal assemblages and exhibits abundant slump structures (Andersen, 1973). This unit is unconformably overlain by late Pliocene shallow-water and tidal deposits, brackish water mudstones and a marine conglomeratic sandstone (Andersen, 1973; Black, 2004).

A notable difference between the Llano El Moreno basin and other rift basins in the Sierra San Felipe is the lack of syn-extensional volcanics. This does not represent a fundamentally different genesis of the basin, but is rather due to its location in between the volcanic fields of the Puertecitos and Sierra Tinaja–Sierra Pinta volcanic provinces (Figs. 2 and 3).

3.2.3. Santa Rosa basin

The Santa Rosa basin is a half-graben composed of late Miocene to Pliocene growth strata and is controlled by the Santa Rosa detachment along its northwestern margin (Fig. 3). The basin is not internally cut by faults with offsets greater than ~100 m and thus constitutes a single tilted and rotated fault block. Sedimentary and volcanic strata in the Santa Rosa basin have inclinations that range from 60° to 10°, however the full range is not observed in any one profile across the basin. Instead, the basin contains systematic along-strike variations in the dip of strata. In the north, the pre-extensional volcanics dip 50–60°, while the youngest syn-kinematic sediments dip 30–40°. In the south, the Tuff of San Felipe dips 20–40° and the youngest basin-fill sediments largely dip less than 25°. The northern portion of the basin is narrower and at a higher elevation, and thus may represent a deeper structural level compared to the southern portion.

A sequence of basement-derived, clast-supported megabreccia deposits overlies the Tuff of San Felipe (~12.6 Ma; Stock et al., 1999) as well as a younger, late(?) Miocene andesite flow (Tma). These megabreccia deposits likely represent the oldest syn-extensional deposits in the basin. This is consistent with the development of a ~5–10° angular unconformity within the lowest syn-rift sediments (<0.5 m above the contact to pre-tectonic Miocene volcanics) in the northeastern portion of the basin, which documents syn-depositional tilting between deposition of the ~12.6 Ma Tuff of San Felipe and a ~6.7 Ma air fall tuff (see below).

Further upsection, a distinctive, non-welded rhyolitic air fall tuff (Tmt) is intercalated within the syn-tectonic sediments. A buff basal horizon with <60% lithics is locally overlain by a purple section with fewer lithics, and both horizons contain abundant sanidine and lesser hornblende phenocrysts in a glass shard matrix. A whole-rock K–Ar age of 16.6 ± 1.3 Ma has been reported for this unit (Bryant, 1986), but new $^{40}Ar/^{39}Ar$ results on K-feldspar suggest a late Miocene age of 6.7 ± 0.2 Ma for this tuff (Seiler, unpublished data). The Santa Rosa basin comprises two other volcanic units (Tmb2, Tmr) within the syn-rift sequence (Bryant, 1986), but geochronological analyses demonstrate that these are much older than the underlying strata and most likely represent megabreccia deposits produced by gravity slides (Seiler, unpublished data).

Lacustrine mudstone and aeolian sandstone deposits overlie the ~6.7 Ma tuff and we interpret them to record the development of a well-established depocentre that may have coincided with faster rates of tectonic subsidence. Further upsection, these fine-grained deposits grade into cobble and boulder conglomerates, which record the return to fluvial sedimentation and the progradation of alluvial fans from the footwall into the basin. The youngest syn-extensional strata dip shallowly to the west and are overlain by subhorizontal Quaternary alluvial fans that post-date the Santa Rosa detachment.

3.2.4. Huatamote basin

Little is known about the syn-rift stratigraphy of the Huatamote basin, which is bound to the west by the Huatamote detachment, as it lacks volcanic deposits that could be used to constrain deposition. Reconnaissance mapping by Oskin (2002) suggests an erosional hiatus between the pre-late Miocene basal sediments (Tos) and the syn-tectonic strata (Tmf) in parts of the southern Huatamote basin. In the north, Pliocene(?) syn-rift sediments of the Huatamote basin lap onto the lower strata of the Santa Rosa basin, which could indicate that extension in the Huatamote basin perhaps post-dates early extension in the adjacent Santa Rosa basin (Oskin, 2002). Further west however, the Pliocene(?) syn-rift strata of the Santa Rosa basin laps onto the basement in the footwall of the Huatamote detachment, which controls the western margin of the Huatamote basin. The mutual onlap between strata of the Santa Rosa and Huatamote basins indicates that there was no significant topographic or structural barrier between the two basins in this region and is not a reliable indication of relative age of the basin-bounding faults.

Fig. 4. Geological map of the northern Sierra San Felipe (simplified from Andersen, 1973; Black, 2004; this study) showing the curvilinear trace of the Las Cuevitas detachment caused by extension-parallel folding and N–S shortening. Anti- and synformal megamullions in the footwall are shown as double-dotted lines with arrows pointing outwards and inwards, respectively. Stereographic projections to the right depict fault–slip measurements of the Las Cuevitas detachment and illustrate primarily extensional and minor oblique- to strike-slip kinematics. West-dipping fault planes in segments 5 and 6 represent tilting of fault planes beyond horizontal. The quality of shear sense is indicated by the shape of arrowheads of the slickenline orientations (full = good, outlined = fair, open arrowhead/V-shaped = poor, no arrowhead = unknown). Calculated compression directions are shown as black circles, intermediate axes as grey squares and extension directions (trend) shown as triangles (black arrows). Faults are dashed were inferred. Cb = Cuevitas basin.

4. Timing of extension

A maximum age for the initiation of extension on the Las Cuevitas detachment is provided by the 19.4 Ma olivine basalt (Tmb1) at the base of the stratigraphy in the Llano El Moreno basin, as well as an undated welded rhyolite tuff that we correlate to the ~12.6 Ma Tuff of San Felipe (Tsf; Table 1). The syn-tectonic sequence of the basin also includes a well-dated sequence of latest Miocene to Pliocene marine rocks (Tpm), which indicate that faulting on the Las Cuevitas detachment must have started prior to ~6–5.5 Ma (Table 1). These stratigraphic relationships are consistent with modelling of apatite fission track and (U–Th)/He data from the footwall of the detachment, which indicates that tectonically induced rapid cooling of the footwall initiated at ~9–8 Ma (Table 1; Seiler, 2009; also Seiler et al., in prep.). The stratigraphic record of the Llano El Moreno basin indicates a shoaling of the basin after ~3.6 Ma, with transition from marine to terrestrial sedimentation occurring during the latest Pliocene (Boehm, 1984). This change in depositional environment may have been caused by decreasing slip on the Las Cuevitas detachment, and faulting is believed to have ceased prior to the deposition of Pleistocene alluvial fans that post-date the Las Cuevitas detachment (Black, 2004).

Onset of extension on the western and central Santa Rosa detachment is bracketed between eruption of a pre-extensional andesite flow (Tma) that overlies the ~12.6 Ma Tuff of San Felipe (Tsf) in the Santa Rosa basin, and the ~6.7 Ma tuff (Tmt) that is intercalated within the syn-rift stratigraphy of the basin (Table 1). This is consistent with apatite fission track and (U–Th)/He data from the footwall of the northeastern Santa Rosa detachment, which shows that accelerated cooling associated with tectonic unroofing there initiated at ~9–8 Ma (Table 1; Seiler, 2009), and indicates that the detachment formed synchronously along its entire length. No Quaternary fault scarps were observed along the detachment and the youngest syn-extensional strata are overlain by subhorizontal Quaternary alluvial fan deposits in a prominent angular unconformity, suggesting that extension on the Santa Rosa detachment ceased during the late Pliocene or early Pleistocene.

The timing of slip on the Huatamote detachment is very poorly constrained. Stratigraphic constraints are inconclusive (see above), and an attempt at dating footwall uplift using apatite fission track analysis was unsuccessful because of the limited amount of rift-related denudation (Seiler, 2009).

In summary, geochronological data indicate that extension began synchronously on the Las Cuevitas and Santa Rosa detachments at ca. 9–8 Ma. The hanging wall basins reached peak subsidence rates in late Miocene–Pliocene time, and extension waned until Pleistocene time when it ceased altogether. Therefore, we interpret the Las Cuevitas and Santa Rosa detachments to have operated together as kinematically linked systems of en-echelon detachment faults. Although little can be said about the onset of extension on the Huatamote detachment, we tentatively suggest that the detachment initiated coevally or shortly after the Las Cuevitas and Santa Rosa detachments, and is likely to have been kinematically linked with the other two detachments over much of the late Miocene–Pliocene.

5. Structural analysis of the Sierra San Felipe fault array

Reconnaissance interpretation of aerial photographs and existing geological maps (Andersen, 1973; Bryant, 1986; Black, 2004) provided preliminary information to guide our field work. On the basis of detailed geological mapping on aerial photographs, rectified from Google Earth™ at a scale ranging from 1:7000 to 1:25,000, as well as standard stratigraphic and structural field methods, we characterised the Neogene fault array of the Sierra San Felipe and identified structures of regional importance.

Displacement estimates for some of the detachment segments were calculated by drawing cross sections parallel to the local extension directions and assuming that: (a) Cenozoic strata were deposited on a subhorizontal basal unconformity that was continuous prior to the onset of late Miocene rifting; (b) strata in the footwall of major faults are less tilted than the strata of the hanging wall, implying that the main faults in the study area flatten with depth; and (c) rollover folds formed in the hanging wall above listric faults. The latter two points are consistent with field observations and allowed us to preserve the conjugate relationship between hanging wall and footwall cut-off angles. The orientation of the nonconformity marker horizon was determined from outcrop inspection and performing a three-point problem on carefully mapped contacts, and projecting the nonconformity towards its intersection with the projection of the detachment. The amount of footwall denudation was matched with modelling results from apatite fission track analysis (Seiler, 2009).

5.1. Structural overview

The Sierra San Felipe fault array contains three left-stepping en-echelon detachment faults (Las Cuevitas, Santa Rosa and Huatamote detachments) and four accommodation zones (Huatamote and Percebu accommodation zones, Cuevitas and Amarillas transfer zones) that relay deformation between the detachments and other faults (Fig. 3). Each of these major structures is composed of a diverse array of individual faults, which can be separated into groups of distinct orientations and kinematics. Our data demonstrate that the Sierra San Felipe fault array consists of three main fault sets: normal faults, dextral strike-slip faults and sinistral strike-slip faults (Fig. 5). Although not abundant, reverse faults are also present in the study area. Normal faults show a wide range of orientations and typically strike NE to NNW, dip from 70° to 20°, and largely accommodate E–SE-down offset (Fig. 5a). Dextral faults show two prominent strike orientations (NW and NNW) and two main inclinations (60–90° and 20–30°; Fig. 5b). Sinistral faults strike predominantly NE–SW with a

Table 1
Initiation of extension on the Las Cuevitas and Santa Rosa detachments.

Type	Age [Ma]	Unit	Comments	Source
Las Cuevitas detachment				
Maximum	19.43 ± 0.47	Tmb1	$^{40}Ar/^{39}Ar$ whole-rock	Esser and McIntosh (2003)
Maximum	~12.6	Tsf	Based on several published K–Ar and $^{40}Ar/^{39}Ar$ ages; fits available data and geological constraints best	See Stock et al. (1999) for compilation of ages
Minimum	~6-5.5	Tpm	Marine microfossils	Boehm (1984)
Onset of denudation	~9–8	Kg	Apatite fission track and (U–Th)/He	Seiler (2009)
Santa Rosa detachment				
Maximum	~12.6	Tsf	Based on several published K–Ar and $^{40}Ar/^{39}Ar$ ages; fits available data and geological constraints best	See Stock et al. (1999) for compilation of ages
Minimum	6.7 ± 0.2	Tmt	$^{40}Ar/^{39}Ar$ on K-feldspar	Seiler (unpublished data)
Onset of denudation	~9–8	Kg	Apatite fission track and (U–Th)/He	Seiler (2009)

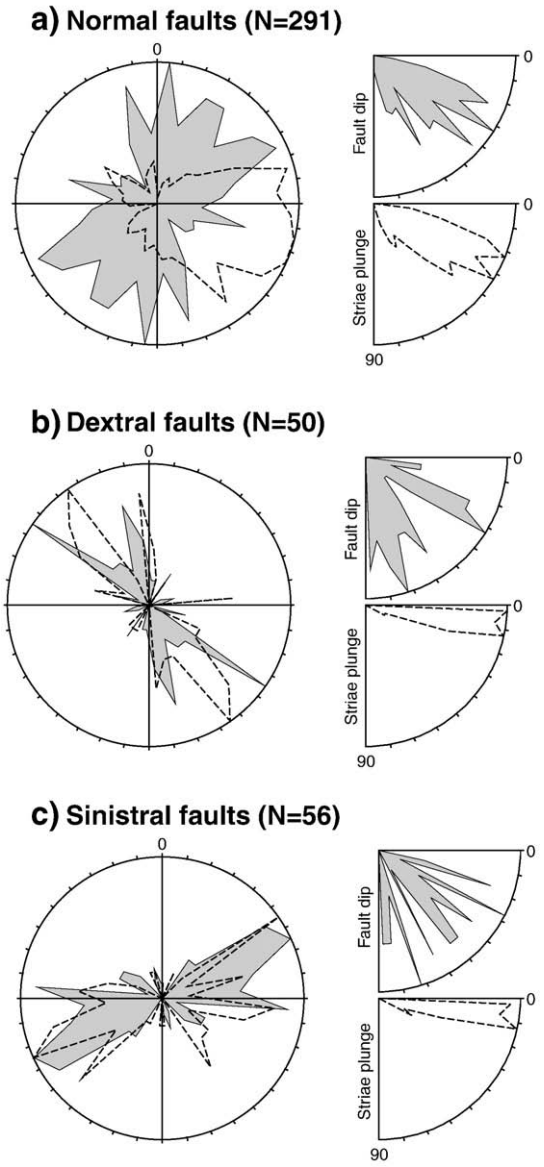

Fig. 5. Rose diagrams depicting the fault array of the Sierra San Felipe. Principal faults are: (a) NNW to NE striking normal faults; (b) NW to NNW striking dextral faults; and (c) NE to E striking sinistral faults, showing highly variable fault dips. Striations (dashed) for normal faults show E- to SE-directed extension in the study area (a), while strike-slip lineations mimic the azimuths of fault planes. (b, c) Strike-slip faults are defined by rakes smaller than 30°.

subordinate peak striking E–W, and exhibit highly variable fault dips (Fig. 5c).

Although fault planes with two or more sets of striations are not uncommon in the study area, clear overprinting relationships were rarely found. Where present, these relationships show no consistent relative age pattern. Out of ten faults that cut the pre-rift stratigraphy and have multiple sets of striae, six were found to record strike-slip preceding oblique-slip movement, two indicate strike-slip after oblique-slip, and two show mutually overprinting striations.

5.2. Detachment faults

The dominant faults in the Sierra San Felipe fault array are a series of three left-stepping detachment faults that control major rift basins as well as many of the modern mountain fronts. They have a highly curviplanar geometry and show strong variations in kinematics and inclination along strike.

5.2.1. Las Cuevitas detachment

The Las Cuevitas detachment is located ~20 km east of the Main Gulf Escarpment where it controls the eastern range-front of the northern Sierra San Felipe (Figs. 3 and 4). The fault extends for ~43 km along strike and juxtaposes west-dipping syn-extensional sediments in the hanging wall against batholithic rocks in the footwall (Black, 2004). The fault is best exposed in the south, which has experienced recent erosion of both the hanging wall and footwall (segments 5–6; Figs. 4 and 6). Further north, the detachment is extensively covered by Quaternary alluvium, but it is exposed in several key outcrops (segments 1–4; Fig. 4). The detachment has a curvilinear trace that defines large-scale fault corrugations or megamullions, the largest of which is a major antiform in the southern portion of the fault (Fig. 4). A stereographic plot reveals that poles to fault planes define a well-developed girdle and demonstrates that megamullion axes plunge to the SE (Fig. 7a).

The Las Cuevitas detachment can be mapped as a single mountain-front fault system, but it exhibits remarkable along-strike variations in orientation and kinematics and thus, has been divided into discrete fault segments (Fig. 4). The most important variation is a systematic decrease in inclination of fault planes, which vary from high and moderate angles in the north (segment 1) to shallow and subhorizontal in the south (segments 5–6; Figs. 4, 8 and 9). In general, the fault segments exhibit normal- to oblique-slip kinematics with minor strike-slip faulting and accommodate east- to southeast-directed extension (Fig. 4). Segments with dip-slip kinematics typically strike north to northeast. Minor strike-slip faulting, usually with a left-lateral shear sense, was observed in all dip-slip segments, but overprinting criteria with dip-slip faults were lacking. A small proportion of the low-angle fault planes measured in segments 5 and 6 dip westwards and exhibit a reverse, east-directed sense of shear. These are likely to represent synthetic secondary fractures or faults that initiated as normal faults and were later tilted beyond horizontal. Striation orientations are highly variable in segments 3 and 5–6, which likely reflects a complicated slip history that may have involved both tilting and vertical-axis rotations of the shear zone.

Fault segment 4 accommodates right-lateral oblique- to strike-slip shearing and facilitates transfer of displacement between the intervening dip-slip fault segments, which form a left-stepping, en-echelon geometry (Figs. 4 and 8). Relatively shallow fault dips in segment 4 may have seen similar tilting as the low-angle segments 5 and 6. The kinematics of segment 2 are poorly understood, but are most likely responsible for the transfer of slip between segments 1 and 3. The presence of a steep escarpment at the southern margin of the syn-tectonic Cuevitas basin (Fig. 4) suggests an approximately E–W oriented right-lateral transfer zone in segment 2. However, E–W oriented fault planes along segment 2 exhibit mostly dip- to oblique-slip striae, and several N–S striking faults record sinistral movement (Fig. 4).

Calculated displacement on the Las Cuevitas detachment increases from ~1.5–1.9 km in the north (segments 1 and 3) to an estimated ~9 km in the southeast (segment 5), pointing to a pronounced southward-increasing displacement gradient on the detachment fault (Fig. 9). In the southernmost segment 6, the detachment significantly changes strike to a more WSW orientation (Fig. 4). Clay gouge, usually well-developed along most of the length of the detachment (Fig. 6), becomes less abundant in the western portion of segment 6. This may suggest that the fault did not accommodate as much slip on the westernmost extreme, perhaps because it is located structurally higher within the fault zone relative to exposures in the eastern portion of segment 6.

Facies changes in late Miocene–Pliocene hanging wall strata are consistent with the proposed displacement gradient that increases systematically from segments 1 to 5 and diminishes toward the west along segment 6. Fluvial sedimentation east of segments 1–3 grades into upper bathyal marine deposits in the hanging wall of segment 5

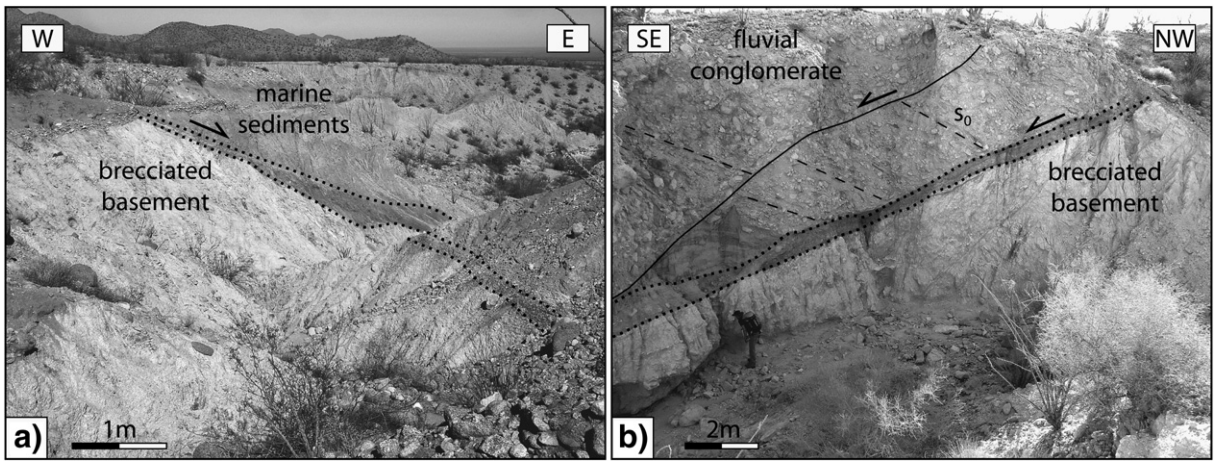

Fig. 6. Photographs of low-angle normal fault exposures of the Las Cuevitas (a) and Santa Rosa (b) detachments. The footwall of the detachments typically exhibits intense fracturing and brecciation in a wide deformation zone (~20–100^{+}m) with abundant secondary fractures and (hydrothermal?) alteration along faults and fractures. Deformation intensity and fragmentation increase towards the main fault plane (dotted line), which is defined by one to two splays of fault gouge (~0.1–5 m) and comprises anastomosing clay gouge zones of up to 65 cm width in a matrix of pulverized basement and minor carbonate veins. Hanging wall strata (dashed line) is much less deformed and dips into the fault plane.

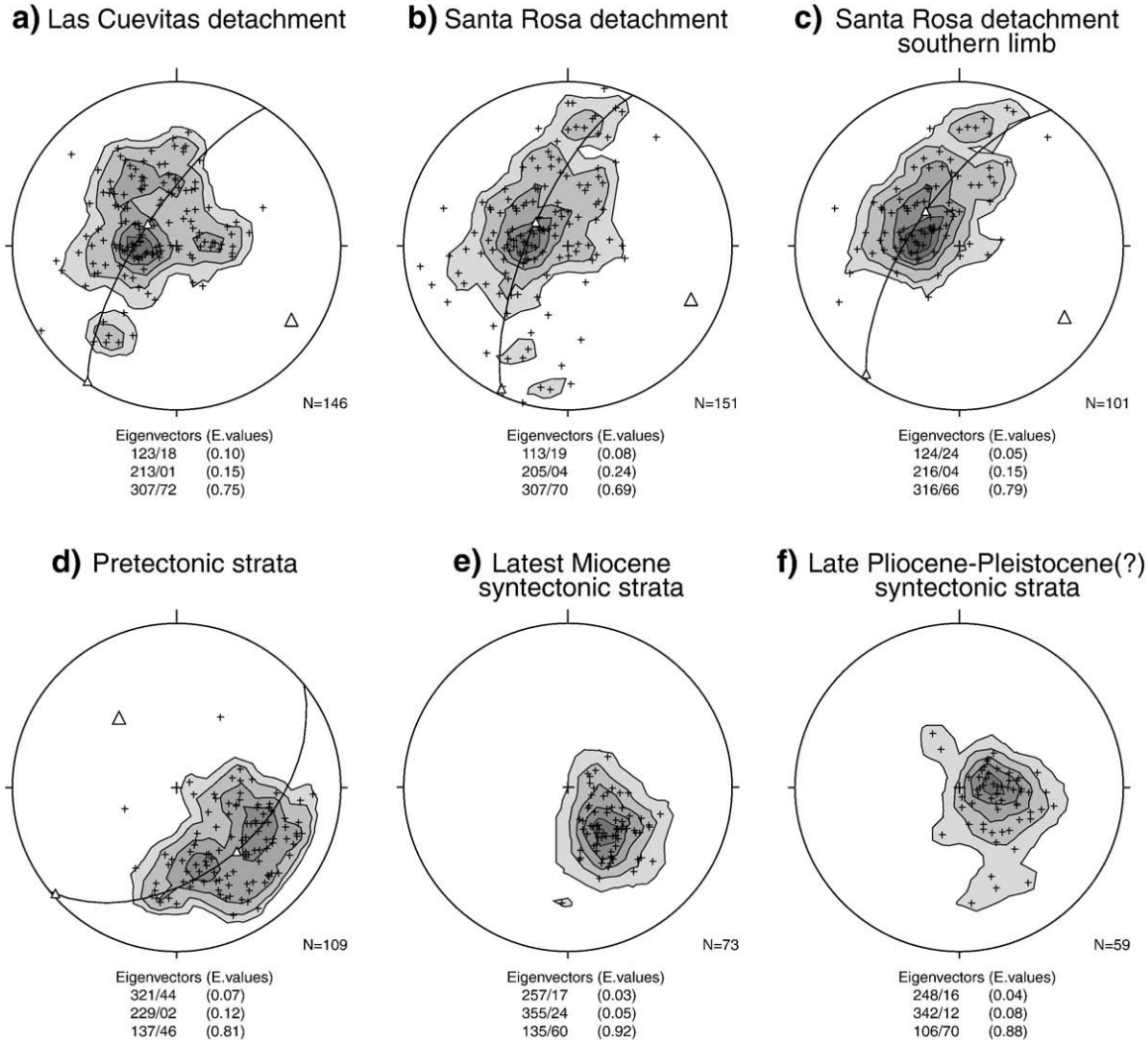

Fig. 7. Stereoplots showing syn-tectonic extension-parallel folding of the Las Cuevitas and Santa Rosa detachments and in the Santa Rosa basin. (a) and (b) show great circle distribution of poles to fault planes from the Las Cuevitas and Santa Rosa detachments. Both detachments exhibit ESE-plunging minimum eigenvectors (fold axes), suggesting comparable folding mechanisms. (c) Same as plot (b) for the southern limb of the antiformal fault corrugation of the Santa Rosa detachment. (d) The weak girdle distribution of the pre-tectonic strata in the Santa Rosa basin documents similar folding as the corresponding detachment segment shown in (c). (e) and (f) show poles to latest Miocene and late Pliocene–Pleistocene syn-tectonic strata of the Santa Rosa basin, respectively. These deposits are significantly less folded than the pre-tectonic strata, implying that constrictional folding initiated during early extension on the Santa Rosa detachment. Much of the across-girdle dispersion is due to differential fault plane shallowing of various detachment segments (a–c) or differential tilting of the hanging wall (d), which explains the relatively low intermediate eigenvalues.

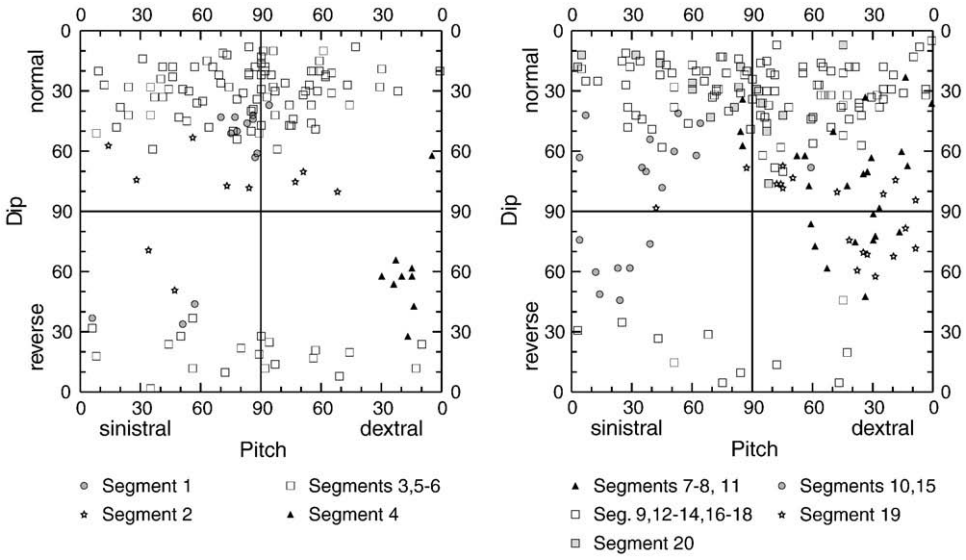

Fig. 8. Dip vs. pitch of the Las Cuevitas detachment (left), and Santa Rosa and Huatamote detachments (right). Detachment faulting is dominated by moderate- to low-angle normal- to oblique-slip faulting (squares) with rare high-angle fault segments (e.g. segment 1). Right-lateral (segments 4, 7–8, 11 and 19) and left-lateral (segments 10 and 15) transfer faults enable strain transfer between en-echelon normal-oblique fault splays.

(Andersen, 1973) that, in turn, change into shallow-water marine and fluvial deposits south of segment 6.

5.2.2. Santa Rosa detachment

The Santa Rosa detachment extends ~36 km along strike, controls the eastern range-front of the central Sierra San Felipe and juxtaposes syn-extensional sedimentary and volcanic rocks with batholithic rocks of the footwall (Figs. 6 and 10). Like the Las Cuevitas detachment to the north, it has a curviplanar geometry defined by a series of megamullion deflections that plunge to the SE (Fig. 7b). Near the prominent antiformal megamullion in the southeastern portion of the central Sierra San Felipe, the fault zone splits into two main splays (Fig. 10). One splay bends to the southwest, forms the northwestern margin of the Santa Rosa basin and comprises the low-angle fault segment originally named Santa Rosa detachment by Bryant (1986). The other splay, the Amarillo fault, continues to the south along the eastern margin of the Sierra Santa Rosa and links with the Amarillas transfer zone (Fig. 10). Geomorphologically, the Amarillo fault defines a very abrupt mountain front, but fault rocks are not exposed along its trace. By contrast, the western strand of the Santa Rosa detachment, located in the footwall of the Amarillo fault (Fig. 11), defines a highly dissected, relict mountain front and is very well-exposed, as is the entire sequence of syn-extensional strata of the Santa Rosa basin (Fig. 10).

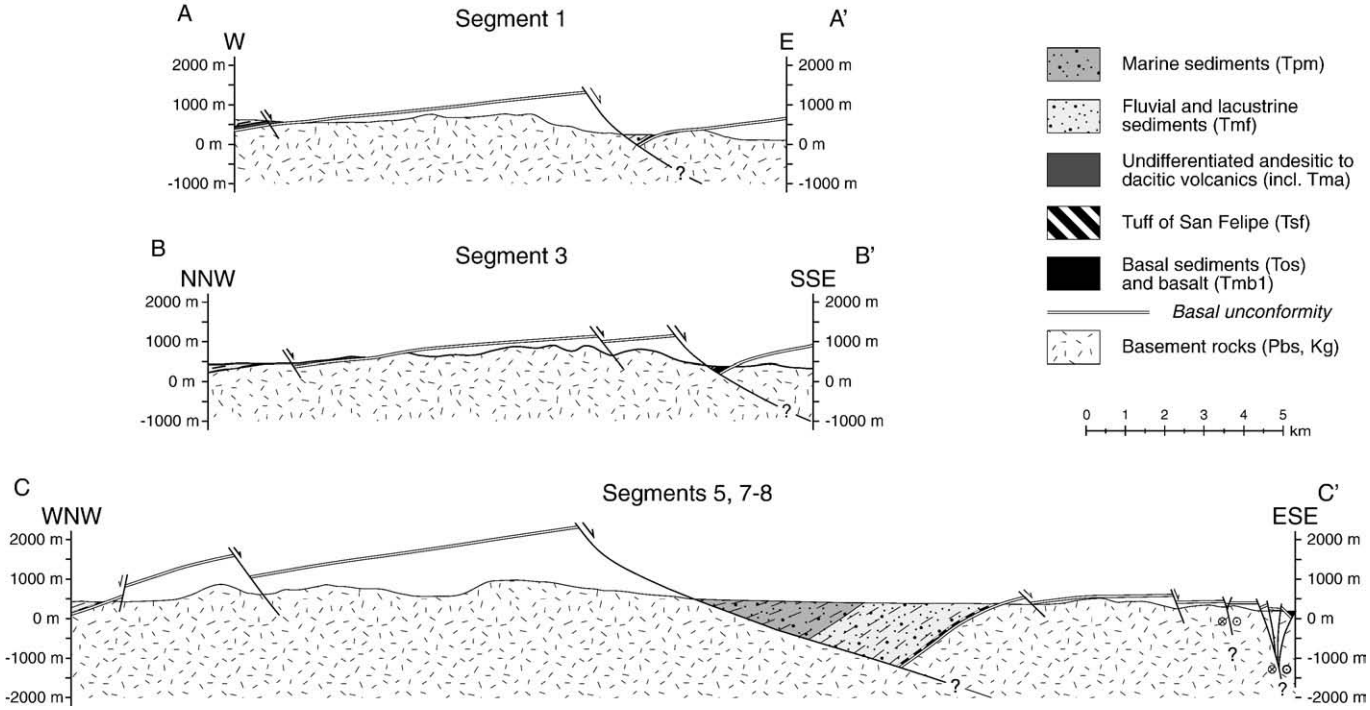

Fig. 9. Schematic cross sections parallel to the local extension direction used to estimate the amount of displacement for selected segments of the Las Cuevitas detachment. Finite displacement for faults cross-cutting crystalline basement rocks is assumed. For locations of sections refer to Fig. 4.

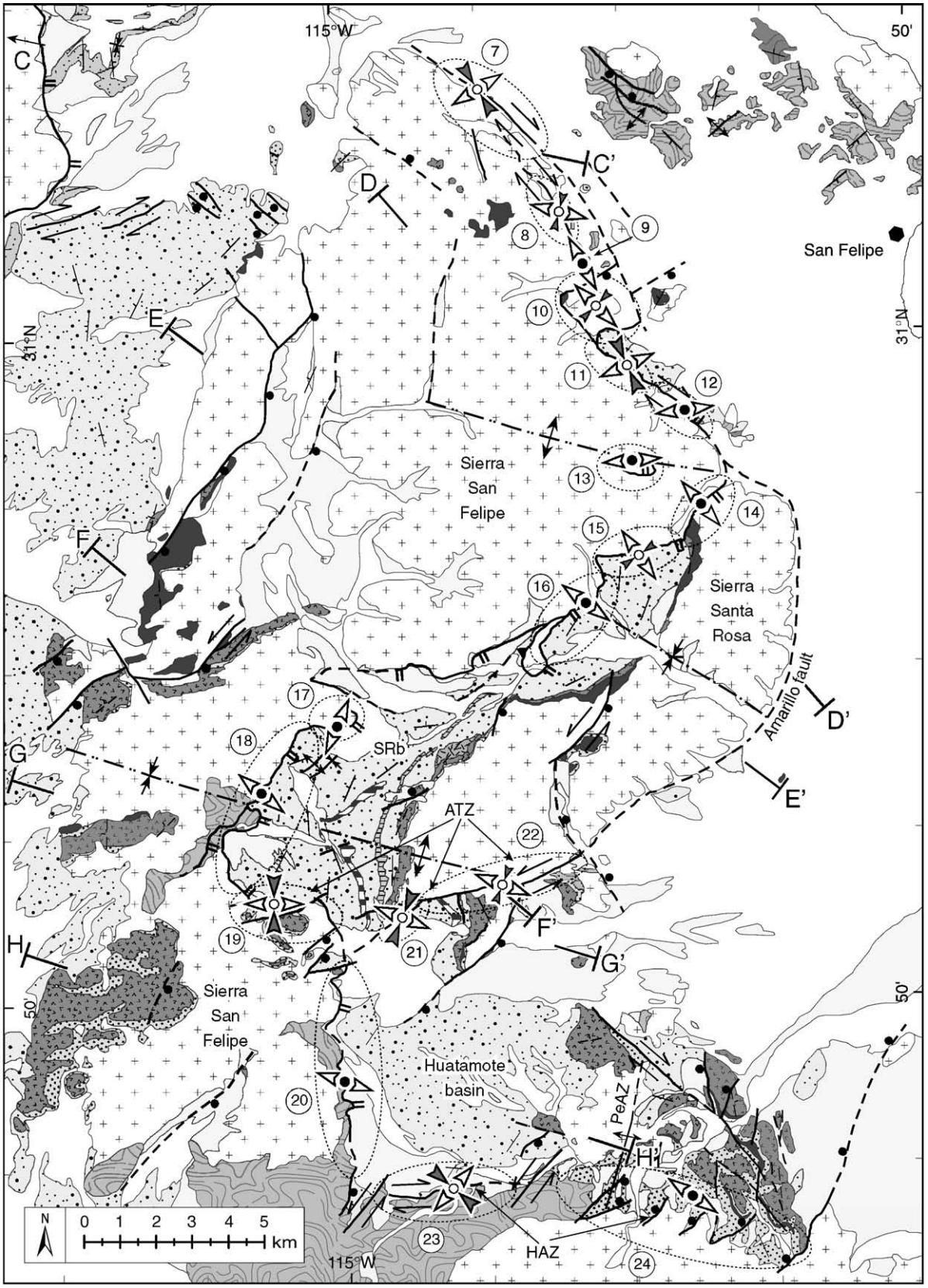

Fig. 10. Geological map of the central Sierra San Felipe and the Sierra Santa Rosa (simplified from Gastil et al., 1975; Bryant, 1986, this study) showing the trace of the Santa Rosa and Huatamote detachments. The fault curvature is thought to represent extension-parallel folding caused by N–S shortening, resulting in syn- and antiformal megamullions (inward and outward pointing arrows) in the footwall (double-dotted lines) and hanging wall (single–dotted lines) of the detachment. Stereographic projections depict fault-slip measurements showing both strike-slip and dip-slip kinematics, with arrowheads indicating the quality of the datum (see caption of Fig. 4). Local stress heterogeneities due to the fault interaction between a transfer fault (segment 19) and the low-angle detachment (segment 18) are thought to have produced atypical ENE–WSW striking dextral faults (dashed great circles in stereoplot 19). Paleostress orientations are shown with compression directions as black circles, intermediate axes as grey squares, and extension directions (trend) marked by triangles (black arrows). Faults are dashed where inferred. ATZ = Amarillas transfer zone, HAZ = Huatamote accommodation zone, PeAZ = Percebu accommodation zone, and SRb = Santa Rosa basin.

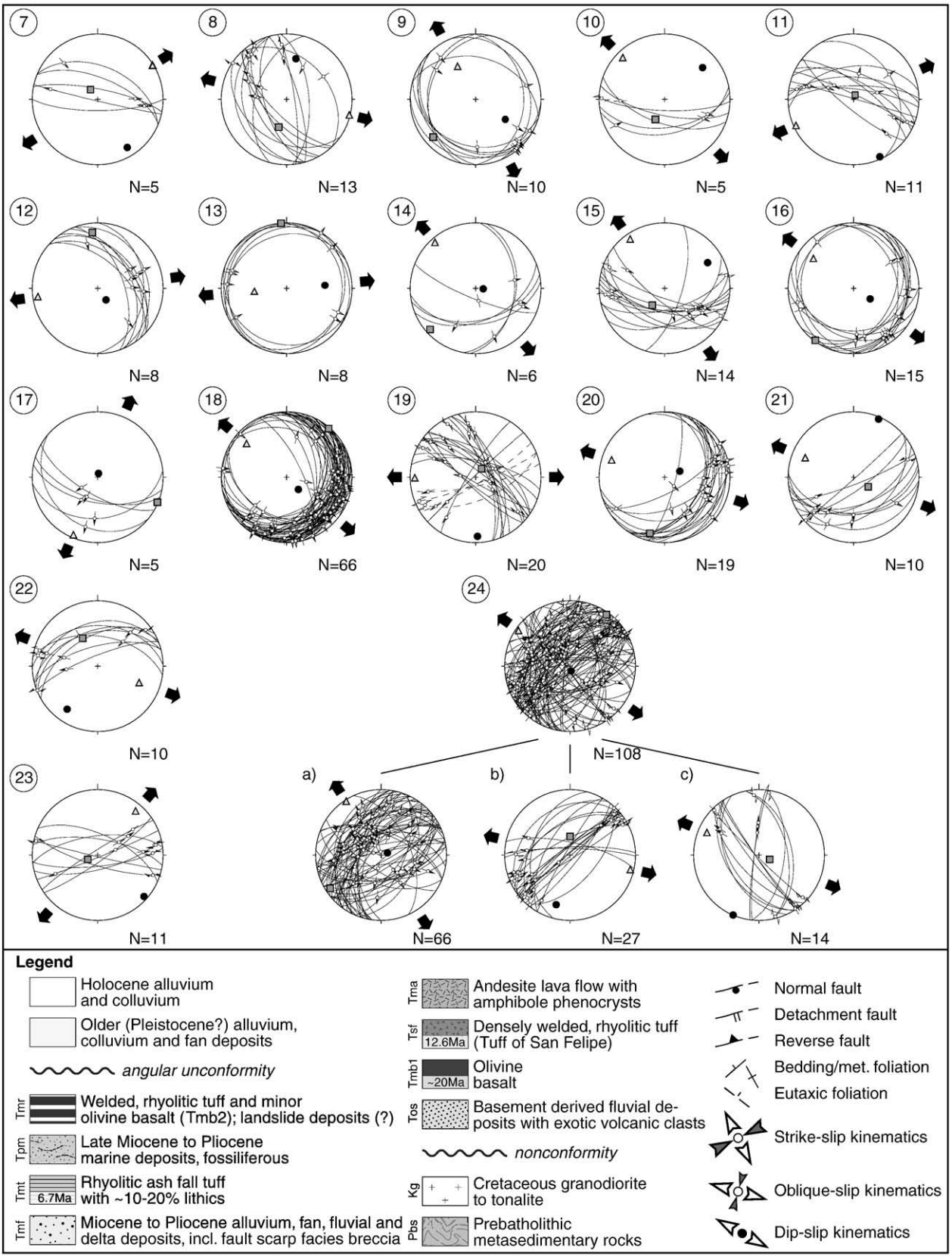

Fig. 10 (*continued*).

Like the Las Cuevitas detachment to the north, the Santa Rosa detachment shows marked along-strike variations in orientation and kinematics, and becomes systematically shallower in inclination toward the south. In the north, the fault zone is composed predominantly of moderate- and high-angle fault planes, whereas southwest of the main bifurcation, the detachment is dominated by

low-angle to subhorizontal fault segments that are connected by much shorter transfer zones with moderately to steeply dipping fault planes (Figs. 8 and 10). Pre-tectonic strata of the Santa Rosa basin have hanging wall cut-off angles of ~50–80° with respect to the Santa Rosa detachment, which indicates that the detachment initiated at high angles and was rotated domino-style to its present moderate- to low-angle orientation.

The northeastern portion of the Santa Rosa detachment (segments 7–13; Figs. 9 and 10) accommodates primarily oblique- to strike-slip with minor dip-slip kinematics (Fig. 8). The principal strike-slip faults (segments 7–8 and 11) accommodate right-lateral displacement and juxtapose basement and Miocene–Pliocene strata to the east against the batholithic basement in the west. In segment 10, two sinistral-oblique faults form in a releasing bend between the two right-stepping dextral faults (Fig. 10). The true amount of displacement in the strike-slip portion of the detachment is unknown, and the finite vertical offset in segments 7–8 is less than ~500 m (Fig. 9). Although poorly constrained, finite displacement in the antiformal megamullion of segments 13–14 is probably ~4.2 km, but may have been as high as ~7.5 km or more if slip on the Amarillo fault is also considered (Fig. 11).

Dextral–oblique displacement in segment 8 occurs within the basement west of the principal fault and exhibits west-dipping fault planes, which could represent either secondary fractures or the eastern half of a negative flower structure (Figs. 9 and 10). Further towards the Sierra Santa Rosa, a slight bend along strike of the same fault plane corresponds to a pronounced change in fault kinematics, from strike-slip in segment 11 to dip-slip in segment 12 (Fig. 10). This suggests that a small change in the spatial orientation of a fault plane may result in fundamentally different kinematics.

West of the main fault, two basement slivers form elevated klippes (segments 9 and 13) above a near-horizontal splay of the detachment fault. Note that both hanging wall and footwall consist of granodioritic basement and thus, these klippes are structurally lower than the mountain-front fault of segments 7, 10–12 and 14 (Fig. 11). The basement klippe of segment 13 lies near the range-crest in direction of mean slip of segment 14 and is likely to have accommodated a substantial amount of slip. Therefore, a significant portion of the slip estimated for segments 13–14 was accommodated on the structurally lower detachment splay of segment 13 (Fig. 11).

The southwestern portion of the Santa Rosa detachment exhibits primarily dip-slip to oblique-slip kinematics and accommodates down-to-the-southeast movement (segments 14–16 and 18; Figs. 8 and 10). Southwestward of the antiformal megamullion, offset structural markers indicate ~5.2 km of slip in the eastern Santa Rosa basin (segment 16), while two well constrained estimates in the central and western portions of the Santa Rosa basin suggest between ~3.8 km (18a) and ~4.7 km (18b) of slip in segment 18 (Fig. 11).

Fault planes in dip-slip segments typically dip at low angles and show variable slickenline orientations (Fig. 8), which is comparable and perhaps genetically similar to the scatter in segments 5–6 of the Las Cuevitas detachment. The oblique- to strike-slip segment 15 defines a left-lateral transfer fault that transfers deformation between right-stepping, en-echelon, dip-slip segments 14 and 16 (Fig. 10). In the central Santa Rosa basin, a basement horse is bound to the east by a SE-dipping low-angle normal fault, while its western margin is defined by a shallowly NW-dipping reverse fault. These faults are interpreted to be part of a single convex-up fault plane, which may originally have defined the upper boundary of a lens-shaped basement sliver, with some fault sections now tilted beyond horizontal. The main splay of the detachment however, lies further north, projects below the horse and does not resurface in the SE.

Segment 17 (Fig. 10) exhibits anomalously steep fault planes with down-dip striae that record either dip- or reverse-slip movement (shear sense was assigned by virtue of contact). This segments exists near a prominent range-front promontory and may have initiated as two conjugate transfer zones.

5.2.3. Huatamote detachment

The Huatamote detachment is defined by a N–S striking low-angle normal fault that controls the prominent escarpment at the western boundary of the Huatamote basin (segment 20; Fig. 10). The detachment is bound to the north and south by the Amarillas transfer zone (segments 19 and 22) and the Huatamote accommodation zone (segments 23–24), respectively. Fault kinematics are dominated by dip- to oblique-slip kinematics with ESE-directed extension. In its hanging wall, the northern part of the Huatamote basin is extensively faulted and shows at least three to four tilted fault blocks that are defined by sinistral-oblique down-to-the-SE faults (e.g. segment 21; Fig. 10). Similar faults are also likely to cut the southern part of the basin (Fig. 11), and are included in a cumulative displacement estimate of ~4.5 km for segment 20, based on offset marker horizons (Fig. 11).

5.3. Accommodation and transfer zones

Four major accommodation and transfer zones serve to accommodate abrupt changes in slip magnitude and transfer deformation between the left-stepping en-echelon detachment faults. Because they are oriented at a high angle to the strike of the detachment faults, they provide an opportunity to evaluate deformation related to the intermediate principal strain axis, which is a component of strain that could not entirely be accommodated on the detachment faults.

5.3.1. Cuevitas transfer zone

The broad area between the northern and central Sierra San Felipe, here referred to as the Cuevitas transfer zone, relays slip from the Las Cuevitas onto the Santa Rosa detachment (Fig. 3). Triangular facets observed along the northern edge of the elevated basin-fill east of segment 6 (Fig. 4) may be related to a WSW–ENE striking dextral(?) fault below the Quaternary alluvium (Black, 2004), with two smaller-scale, dextral faults possibly representing Riedel faults. However, we have not studied the Cuevitas transfer zone in detail and the exact characteristics of this zone remain unresolved.

5.3.2. Amarillas transfer zone

The Amarillas transfer zone is a synthetic transfer fault that forms the southern margin of the Santa Rosa basin (segments 19 and 22; Fig. 10). This fault defines the topographic escarpment that continues along the southern margin of the Sierra Santa Rosa and merges with the Amarillo fault, the southeastern strand of the Santa Rosa detachment (Fig. 10).

The transfer zone exhibits complex kinematics that change markedly along strike. In its western portion (segment 19), the E–W striking transfer zone accommodates dextral–oblique slip (Fig. 8) and juxtaposes Miocene basin-fill in the north against Cretaceous plutonic basement and Paleogene sediments to the south (Fig. 10). A subordinate ENE–WSW striking left-lateral fault, which cross-cuts and thus post-dates the right-lateral transfer zone, overprints the contact between basement and Paleogene sediments to the south of segment 19 and is interpreted to have initiated during later stages of deformation.

Near the intersection with the Huatamote detachment to the south, the strike-slip component of shear across the Amarillas transfer zone changes from dextral in the west (segment 19) to sinistral in the east (segment 22; Fig. 10). The eastern portion of the fault zone dips steeply to moderately to the north and juxtaposes batholithic basement against syn-extensional Miocene–Pliocene strata in the south (Figs. 10 and 11). Note that restoration of northwest tilted strata along the northwestern Sierra Santa Rosa would rotate this fault segment to an even shallower dip to the north (segment 18b; Fig. 11). Therefore, sinistral shear of this segment of the transfer zone must have included a substantial component of reverse movement that amounts to ~600 m based on offset rock units (segment 18a; Fig. 11). Importantly, this reverse movement is most prominently developed

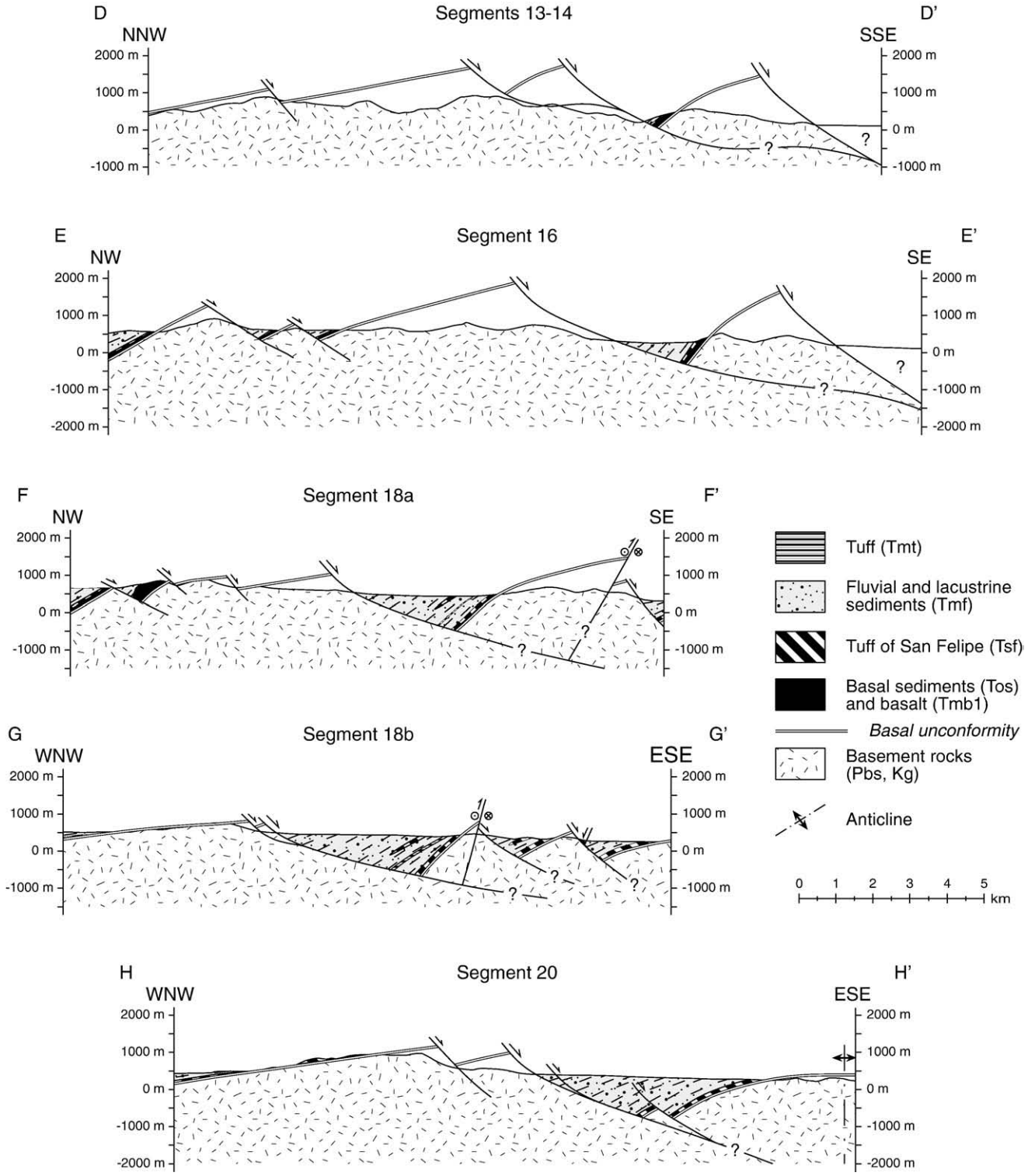

Fig. 11. Schematic cross sections parallel to the local extension direction (for locations of sections refer to Fig. 10). The sections were used to estimate the amount of displacement for portions of the Santa Rosa and Huatamote detachments. Finite displacement is assumed for faults that juxtapose crystalline rocks only.

in the lower syn-rift deposits of the Huatamote basin, whereas no reverse faults were observed that cut the upper part of the stratigraphy further west along the transfer zone. This suggests that sinistral-reverse movement occurred progressively with extension, but the exact timing when slip on the Amarillas transfer zone initiated is not well constrained.

Strain patterns in the area of shear sense reversal are more complicated than elsewhere along the Amarillas transfer zone. The thickness of clay gouge decreases from ~20–30 cm in segments 19 and 22, to <5 cm in the region of the polarity reversal, which likely indicates diminished fault displacement. This segment of polarity reversal coincides with the region of mutually onlapping sediments from the Huatamote and Santa Rosa basins, which is consistent with the lack of a prominent topographic and structural barrier as inferred from decreasing fault displacement on this portion of the transfer zone. Deformation in this middle segment is not only taken up by

faulting, but also by small-scale chevron folding of Pliocene(?) syn-extensional strata. The moderately N-plunging fold axes and west-dipping axial planes of these folds indicate E–W contraction, which conflicts with the inferred regional kinematics and is more likely related to local shortening oblique to the strike of the Amarillas transfer zone.

5.3.3. Huatamote accommodation zone

The Huatamote accommodation zone separates the strongly dissected Huatamote basin from the relatively intact basement to the south and is responsible for broad right-lateral shear (segments 23–24; Fig. 10). In its western portion (segment 23), an E–W striking, dextral–oblique transfer zone juxtaposes late Miocene(?)–Pliocene basin-fill to the north against metasedimentary basement in the south. Further east (segment 24), a series of closely spaced faults with small to moderate offsets (hundreds of meters) disrupt the pre-rift sedimentary (Tos) and volcanic strata (Tmb1, Tsf) of the southern Huatamote basin (Fig. 10). Faults vary from moderately NW- and SE-dipping normal faults to steeply dipping, conjugate sinistral and dextral strike-slip faults.

Most faults in the Huatamote accommodation zone are hinge faults that diverge to the north and die out toward their southwestern ends (Fig. 10). Pairs of faults with opposing senses of shear have V-shaped intersections and likely accommodate extension that increases northward within the accommodation zone, thereby effectively facilitating right-lateral shear.

5.3.4. Percebu accommodation zone

The Percebu accommodation zone is located near the eastern limit of the Huatamote basin, where the exposed basement defines the hinge of a broad NNE–SSW oriented anticline between systematically W-dipping strata to the west and E-tilted strata to the east (Fig. 10). This type of accommodation zone is classified as a strike-parallel, antithetic accommodation zone and is thought to form between two macroscopic conjugate faults that dip towards each other (Faulds and Varga, 1998; Faulds et al., 2002). While the Huatamote detachment (segment 20) is the obvious candidate for the western bounding fault, a similarly prominent fault to the east is lacking (Fig. 10). We propose that a moderately NW-dipping normal fault in the southeastern portion of the study area, which juxtaposes Paleogene to Pliocene(?) strata in the hanging wall against batholithic footwall basement, acts as the western boundary of the Percebu accommodation zone (Fig. 10). Except for the southwestern extreme however, both fault and footwall are extensively covered by Quaternary alluvium, which impedes a rigorous evaluation of the relative importance of this fault. Alternatively, this fault may be part of a much larger down-to-the-west fault zone related to the Cañon El Parral fault zone or the structurally lower Ironwood Canyon detachment (Fig. 3), both of which are west-directed normal faults in the Sierra San Fermín to the southeast (Lewis and Stock, 1998a).

The faults that most likely control the Percebu accommodation zone (the Huatamote detachment in the west and any of the three potential faults in the east) have a ~30–45° misalignment in strike that causes them to diverge towards the north (Figs. 3 and 10). This geometry likely represents a northward increasing displacement gradient on both faults, which results in vertical-axis rotations that accommodate dextral shear (Fig. 10). A northward increasing strain gradient in the Huatamote basin is consistent with the kinematics of the smaller-scale hinge faults of the Huatamote accommodation zone.

6. Kinematic analysis and paleostress orientations

6.1. Methodology

Kinematic analysis and paleostress calculations, based on a total of 501 fault-slip measurements, were carried out separately for all fault segments. Each fault-slip datum consists of the measured fault plane, movement direction, shear sense (where possible), and a quality factor assessing the reliability of the datum. Separation into geographical areas was necessary because the main structures of the study area represent a complex fault array with diverse kinematics on variably oriented fault planes. For initial data evaluation after geographical grouping, we examined the fault-slip data in stereographic plots, and the faults in the study area were divided into segments that displayed internally consistent and compatible kinematics.

Paleostress axes were calculated for each fault-slip datum. The maximum and minimum compressive paleostress axes were assumed to lie within a plane defined by the striae and the normal to the slip surface, and inferred to form angles of 30° and 60°, respectively, with respect to the slip surface in a manner that is consistent with the Mohr–Coulomb shear failure criterion. The intermediate principal paleostress axis lies perpendicular to the other two and is oriented parallel to the slip surface and perpendicular to the striae. Integrated paleostress axes were calculated using linked Bingham statistics (Bingham, 1964) on all slip data in each fault segment (Figs. 4 and 10). In order to simplify the kinematic description of fault segments, we refer to the maximum and minimum integrated paleostress directions as shortening and extension axes.

Fault segments were classified into kinematic regimes based on the Anderson theory of faulting, where high-angle shortening axes ($\geq 60°$) and low-angle extension axes ($\leq 35°$) were classified as dip-slip, normal kinematic regimes. A relatively high threshold for the maximum inclination of the extension axis was chosen because some fault segments have experienced significant domino-style tilting. Strike-slip kinematics were assigned to fault segments with steep intermediate axes ($\geq 65°$), whereas oblique-slip kinematics were attributed to fault segments with moderately inclined intermediate axes (21–64°). Three of the 24 calculated paleostress orientations that correspond to fault segments 6, 9 and 13 clearly accommodated dip-slip, but failed meet the above criteria due to a substantial amount of tilting and shallowing of the fault.

6.2. Reconstructed paleostress orientations

Integrated paleostress directions on the Las Cuevitas detachment exhibit primarily extensional kinematics with minor oblique- to strike-slip movement (Fig. 4, Table 2). The computed extension direction varies significantly along strike of the detachment fault, from ENE- to NNE-directed extension in the north (segments 1–2), to E-directed extension in the central portion (segments 4–5), and SE-directed extension in segments 3 and 6 (Fig. 4, Table 2). The extension axes are subhorizontal in the northern portion of the detachment (segments 1–3), but plunge shallowly to the WNW in southern segments 4–6 (Fig. 4). This likely reflects the change in inclination of the Las Cuevitas detachment from moderate angles in the north to low angles in the south. The orientations of compressive stress axes depend primarily on the kinematic regime of the respective fault segment. In extensional segments, the shortening axis is either near-vertical (segments 1 and 3), or moderately to steeply inclined (segments 5–6), while oblique to strike-slip segments (segments 2 and 4) exhibit shallowly plunging to subhorizontal shortening axes (Fig. 4, Table 2).

Paleostress calculations in the northeastern section of the Santa Rosa detachment reveal NE to E oriented extension directions in a dominantly strike-slip kinematic regime with subordinate extension (segments 7–8 and 11–13; Fig. 10, Table 2). The integrated extension axis is oriented SE to SSE in sinistral step-over segments (segments 9–10; Fig. 10), which differs markedly from adjacent segments. In general, extension axes are subhorizontal in the northern Santa Rosa detachment (segments 7–8 and 10–12). Only the two tectonic klippes in the footwall (segments 9 and 13) show extension axes

Table 2
Results of paleostress calculations of the Las Cuevitas, Santa Rosa and Huatamote detachments.

Fault Segment	Number of data	Shear sense indicators[a]	Compression axis		Intermediate axis		Extension axis		Kinematic regime
			Trend	Plunge	Trend	Plunge	Trend	Plunge	
1	15	s-c, R	349	70	165	20	255	1	Extension
2	10	s-c, R, contact	301	39	103	49	203	9	Oblique
3	24	R, contact	101	84	236	4	327	4	Extension
4	11	s-c, R	174	12	68	52	272	36	Strike-slip
5	40	Contact	106	63	13	2	282	27	Extension
6	57	Contact	108	54	220	15	319	32	Extension[b]
7	5	R	148	15	324	75	58	1	Strike-slip
8	13	s-c	13	36	196	54	104	2	Oblique
9	10	s-c	124	44	228	14	332	42	Extension[b]
10	5	s-c, strain shadow	50	25	205	62	315	10	Oblique
11	11	s-c, R, R′, T, strain shadow, contact	155	4	20	84	246	4	Strike-slip
12	8	s-c, R, contact	144	72	354	16	262	9	Extension
13	8	R, P, T	86	41	355	0	265	49	Extension[b]
14	6	R	93	81	228	7	319	7	Extension
15	14	s-c, s-c′, R, contact	59	24	216	64	325	9	Oblique
16	15	s-c, R, slickenfibres, contact	123	65	216	2	307	25	Extension
17	5	Contact	12	85	113	1	203	5	Extension
18	66	s-c, R, dragged bedding, contact	137	69	41	2	310	21	Extension
19	20	s-c, s-c′, R, R′, T, contact	178	10	35	77	270	8	Strike-slip
20	19	R, contact	68	70	195	12	288	16	Extension
21	10	s-c, R, contact	23	4	123	68	292	21	Strike-slip
22	10	R, contact	215	20	331	50	111	33	Oblique
23	11	R, T, contact	132	5	246	77	41	12	Strike-slip
24	108	s-c, R, T, slickenfibres, groove marks, dragged/offset strata, contact	167	84	35	4	305	5	Extension

[a] R, R′, P and T as described by Petit (1987).
[b] Manually assigned kinematic regime (see text).

plunging at ~40–50°, which is likely related to block tilting and fault plane shallowing in these segments (Fig. 10, Table 2).

The Santa Rosa detachment southwest of the main bifurcation is dominated by extensional and minor strike-slip kinematics, and extension axes are oriented SE and ESE (segments 14–16 and 18; Fig. 10, Table 2). The integrated kinematics of segment 17 yield NNE- or SSW-directed extension, which differs markedly from other segments of the southern Santa Rosa detachment but, as mentioned earlier, this is an anomalous segment that overall transfers slip in a short step-over of the main detachment.

The Huatamote detachment (segment 20) to the south is dominated by extensional kinematics with a SE oriented extension axis (Fig. 10, Table 2). Like the southern portion of the Santa Rosa detachment, the integrated extension axis of the Huatamote detachment is moderately inclined due to block tilting and fault-plane shallowing.

The Amarillas transfer zone yields extension axes oriented E to SE (segments 19 and 21–22; Fig. 10, Table 2), which is similar to the calculated extension directions of adjacent detachment segments to the north and south (i.e. segments 18 and 20). Shortening axes vary from shallow to moderately inclined as the kinematic regime changes from strike-slip in the west to oblique-slip in the east (Fig. 10).

The Huatamote accommodation zone has two distinct segments with marked differences in paleostress regimes (Fig. 10). The western segment 23 accommodated dextral strike-slip with NE-directed extension and a subhorizontal NW oriented shortening axis. The complex fault pattern of the eastern Huatamote accommodation zone (segment 24) has initially been split into three kinematic subsets: (a) most fault planes strike NE–SW and are high-angle faults with normal to oblique (sinistral and dextral) shear sense (segment 24a; Fig. 10); (b) lesser NE–SW striking, steeply dipping sinistral faults (segment 24b; Fig. 10); and (c) conjugate NNW–SSE striking dextral fault planes (segment 24c; Fig. 10). However, overprinting relationships amongst the three subsets are inconsistent, with dip- and strike-slip faults mutually overprinting. Moreover, all three subsets are dominated by subhorizontal SE-trending extension axes and are kinematically compatible in a scenario where the intermediate and shortening directions alternate. The change in kinematics between segments 23 and 24 coincides well with the intersection of the Percebu accommodation zone and the inferred change to NW-directed normal faulting in the eastern Huatamote basin (Fig. 10).

7. Temporal and spatial analysis of fault kinematics

Paleostress orientations vary significantly within the Sierra San Felipe fault array, and these variations are crucial to evaluate the tectonic models for the evolution of the Gulf of California. Fig. 12 shows that the fault population can be divided into two groups of faults with broadly ENE and SE-trending extension axes. Similar patterns of (E)NE- and SE-directed extension have been recognised elsewhere in the Gulf Extensional Province, where the two extension directions have been interpreted to represent temporal changes in the stress field associated with the transition from proto-gulf orthogonal rifting to the modern phase of transtensional shearing as proposed by the two-phase model of rifting. If this model also applies to the study area, one might expect the faults with NE-trending extension axes (Fig. 12a) to have formed during the proto-gulf phase, and faults with SE-trending extension axes (Fig. 12c) to have formed during the modern phase. However, such artificial grouping of faults does not correlate with the age of strata cross-cut by the faults. Instead, our mapping shows that a single fault with the same cross-cutting relationships records marked variations in kinematic axes along strike (e.g. segments 4–5, 11–12 and 14–16). Many of the radical changes in kinematics are associated with jogs and steps in the main fault plane, but equally profound variations are associated with major changes in the macroscopic geometry of the faults around megamullions. The kinematics of faulting in accommodation and transfer zones are strongly controlled by relative slip rates of the detachments that they link together, and thus add additional complexities to the analysis.

A hypothetical temporal control on fault kinematics can be tested in the well-exposed Santa Rosa and Huatamote basins (Fig. 10) using fault arrays that cut different sections of the hanging wall within a single fault segment. Fig. 13 shows several temporally filtered subsets of faults. The oldest category of faults includes those that cut pre-rift

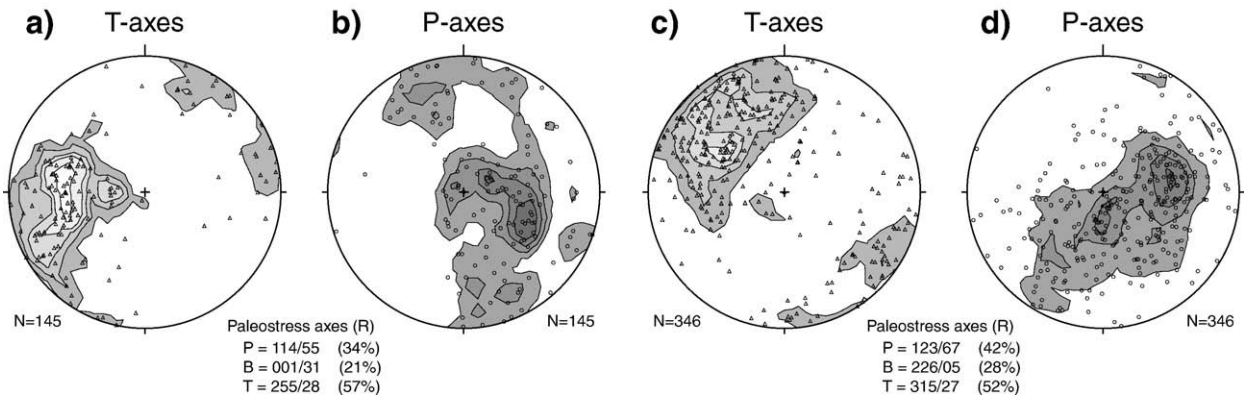

Fig. 12. Contour plots of P- and T-axes calculated for all fault-slip data of the study area, but separated with respect to ENE- (a, b) or SE-directed (c, d) extension. The T-axes scatter around a WSW (a) or NW (c) maximum, respectively, showing relatively broad peaks due to vertical-axis rotations and/or extension-parallel folding. P-axes show a girdle distribution with a vertical maximum, and a significant component of approximately N–S (b) to NE–SW (d) horizontal shortening. R = Regelungsgrad (distribution parameter where 0% = homogeneous distribution and 100% = parallel fabric; Wallbrecher, 1986).

stratigraphy such as the Tuff of San Felipe and other volcanic and sedimentary rocks found near the nonconformity (Fig. 13b, d and f). These faults are compared to the fault-slip data from the respective segment of the detachment faults (Fig. 13a, c and e), which we take as a proxy for young fault slip. This may not strictly hold true, as detachment faults obviously record both relatively old (proto-gulf) and young (Pliocene) movement. However, we believe such an approach is warranted because: (a) significant tilting indicates that fault slip must also have occurred during/after deposition of late Pliocene syn-extensional hanging wall sediments; (b) later fault movement will overprint and partially obliterate earlier striations, thus decreasing its influence on the paleostress reconstruction; and (c) hanging wall geometries and the orientation of basin-fill sediments are broadly consistent with the reconstructed paleostress orientation of the respective fault segment, indicating that late fault movement is compatible with the calculated paleostress orientation.

The extension direction for all of these fault subsets varies in azimuth from 286° to 310°, but does not show any systematic variation that correlates with the age of the cross-cut strata. In fact, virtually the entire range of extension directions is represented in each of the three detachment subsets (Fig. 13a, c and e), which cross-cut strata of the same age but are located in different segments of the detachment system. We therefore interpret these data to demonstrate that spatial variations in fault kinematics are more important than temporal variations, which is consistent with the earlier observation of mutual overprinting between multiple sets of striae throughout the study area.

8. Constrictional strain in the Sierra San Felipe

8.1. Observations from fault kinematics

Paleostress axes from all of the faults in the study area clearly demonstrate the constrictional nature of strain accommodated by the fault network of the Sierra San Felipe (Fig. 12). Constrictional strain is characterised by prolate (cigar-shaped) finite strain ellipsoids, which is produced by radial shortening perpendicular to a dominant extension direction. Both kinematic subsets with NE and NW oriented extension axes exhibit a well-developed great circle distribution of shortening axes (Fig. 12b, d), which is compatible with constrictional strain.

Multiple directions of tectonic shortening are also observed at a macroscopic scale within the fault array. All of the principal faults are dominated by segments that accommodate up to ~9 km of normal displacement. Slip on these faults results in significant crustal thinning, and we therefore infer that the maximum finite shortening axis is vertical. However, the study area also exhibits several reverse faults that generally strike E–W, the most prominent being the eastern portion of the Amarillas transfer zone. These faults indicate a component of subhorizontal shortening in a N–S orientation, which we interpret to represent the nature of strain along the intermediate finite strain axis.

8.2. Megamullions and extension-parallel folding

Large-scale fault plane corrugations or megamullions of the Las Cuevitas and Santa Rosa detachments provide further evidence for the character and evolution of finite strain accommodated by the San Felipe fault array. Both detachments are broadly warped into antiformal and, in case of the Santa Rosa detachment, synformal megamullions that have a half-wavelength of ~15–20 km and amplitudes of ~4–7 km (Figs. 3, 4 and 10). The detachments also show a range of smaller-scale undulations with wavelengths as short as ~1–2 km. Poles to fault planes are distributed about a great circle that defines the shallow, SE-plunging orientation of the macroscopic axes of the megamullions (Fig. 7a, b). The strong similarity in orientation of the macroscopic axes indicates that the megamullions of both detachments likely formed due to similar processes.

Genetic end-members used to explain the formation of extension-parallel megamullions include: (a) grooves or corrugations of originally non-planar fault surfaces; (b) displacement-gradient folds, which represent the bending of fault surfaces in response to differential isostatic uplift caused by along-strike displacement gradients; and (c) constrictional folds due to horizontal shortening perpendicular to the regional extension direction (Spencer, 1984; John, 1987; Yin and Dunn, 1992; Fletcher and Bartley, 1994; Mancktelow and Pavlis, 1994; Fletcher et al., 1995; Schlische, 1995; Janecke et al., 1998; Spencer, 2000). Field relations in the San Felipe fault array demonstrate that all three of these end-members operated together to produce the observed macroscopic geometry. A fourth mechanism of continuous casting has been proposed for faults that develop in high-T brittle or ductile regimes (Spencer, 1999), but can be discarded as a viable process given low pre-extensional paleo-temperatures in the Sierra San Felipe (Seiler, 2009).

Numerous fault segments (e.g. segments 2, 10, 15 and 17) form step-overs that connect misaligned strands of both the Las Cuevitas and Santa Rosa detachments, which clearly demonstrates that the faults formed with an originally non-planar geometry. Although not studied in detail, similar processes are also likely to be responsible for the scalloped surface trace of the San Pedro Mártir fault (Figs. 2 and 3). In addition, the megamullions on the Las Cuevitas and Santa Rosa detachments are thought to have attenuated by other processes.

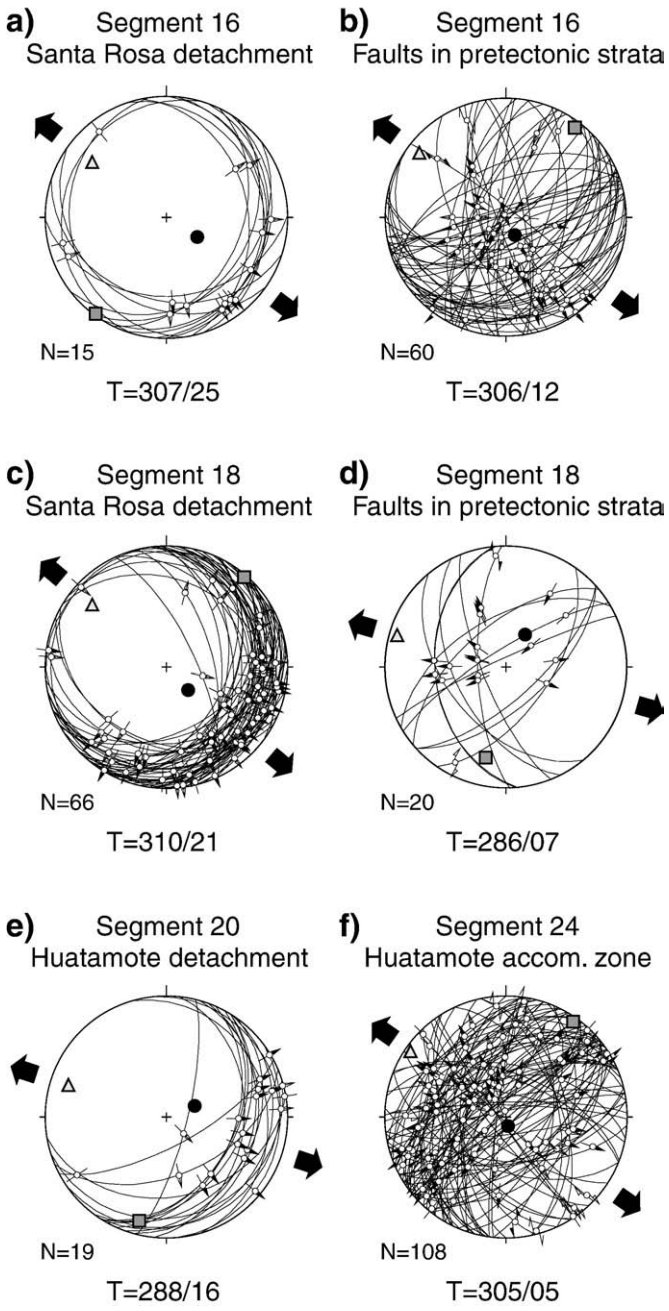

Fig. 13. Fault-slip data of (a) Santa Rosa detachment in segment 16; (b) the pre-rift stratigraphy in the hanging wall of segment 16; (c) the detachment fault in segment 18; (d) the pre-6.7 Ma stratigraphy east of fault segment 18; (e) the Huatamote detachment in segment 20; and (f) the pre-rift stratigraphy of the Huatamote accommodation zone (segment 24). Comparison between faults that cut pre-rift strata (right) with the corresponding detachment segment (left) does not show any systematic variation of the extension direction between fault arrays that were active during the proto-gulf and modern stress regimes, respectively. Paleostress orientations are shown with compression directions as black circles, intermediate axes as grey squares, and extension directions marked by triangles.

Firstly, the curvature of the two detachments is significantly higher than that of the Main Gulf Escarpment and secondly, megamullions of the Las Cuevitas and Santa Rosa detachments show no correlation in either location, wavelength, or amplitude with the corrugations of the San Pedro Mártir fault (Fig. 3).

Both detachment faults accommodated major along-strike displacement gradients, which would be expected to generate along strike variations in isostatic rebound of the footwall. This seems to be consistent with an apparent correlation between a major antiformal corrugation on the Las Cuevitas detachment in segment 5 and the location of a deep synclinal basin in its hanging wall as inferred from an upper bathyal depositional environment compared to fluvial deposition further south and north (Figs. 4 and 9). In the case of the Santa Rosa detachment, the axial surfaces of the antiformal and synformal megamullions do not coincide with the locations of maximum and minimum fault slip, respectively (Figs. 10 and 11). Rather, finite displacement reaches a maximum (~5.2 km) just south of the antiformal hinge, and remains more or less constant (~3.8-4.7 km) along the southern limb and in the synformal hinge zone (Figs. 10 and 11). Therefore, we interpret that other processes such as the accommodation of constrictional strain are required to explain the observed macroscopic geometry of the Santa Rosa detachment. Given the above mentioned similarity between the orientation of the megamullion axes of the Santa Rosa and Las Cuevitas detachments (Fig. 7a, b), it likely that the latter has also accommodated constrictional strain.

Syn-extensional strata of the Santa Rosa basin show key structural relationships which demonstrate that megamullions amplified as constrictional folds synchronously with the onset of slip on the Santa Rosa detachment. One crucial observation is that axial surfaces of megamullions in the footwall largely coincide with axial surfaces of folds in the overlying hanging wall (Fig. 10). However, as a consequence of their opposing dip directions, synformal (antiformal) megamullions of the east-dipping detachment coincide with antiformal (synformal) folds of the west-dipping strata (Fig. 10). Because the folded stratigraphic markers in the hanging wall formed synchronously with slip on the detachment, they provide critical relationships to evaluate when the folding began. The poles to fault surfaces from segments of the detachment that bound the Santa Rosa basin (segments 14–18) exhibit a moderately developed girdle distribution, which defines a best-fit axis of the megamullions that plunges with 24° to an azimuth of 124° (Fig. 7c). As this subset is derived from only the southern limb of the major antiformal megamullion, the girdle is not as well-developed as in the data set of fault surfaces from the entire Santa Rosa detachment (Fig. 7b). Poles to pre-extensional strata of the Santa Rosa basin also have a weak girdle distribution with a best-fit fold axis that plunges 44° towards an azimuth of 321° (Fig. 7d). The strong similarity in azimuth of the fold and megamullion axes is consistent with their formation as upright constrictional folds. The eigenvalues of the poles to the detachment and pre-extensional strata are also very similar, which strongly suggests that both have experienced the same degree of folding (Fig. 7c, d). The girdle is slightly better developed in the detachment data set, which we interpret to be largely due to the greater heterogeneity in orientation of the fault surfaces as well as original grooves in the detachment surface. By contrast, the poles to the syn-extensional strata do not define girdles, and minimum eigenvectors do not coincide with the NW–SE orientation of the axial surface of megamullions and folds in the pre-extensional strata (Fig. 7e, f). Even though mapping clearly shows that the younger syn-extensional strata are also folded (Fig. 10), the poles to stratification indicate that they are much less folded than either the detachment fault or the pre-extensional strata. These relationships conclusively demonstrate that constrictional folding started at the earliest stages of faulting and occurred throughout the entire history of slip on the detachment, which is consistent with the one-phase kinematic model of integrated transtensional deformation in the Gulf Extensional Province.

9. Rotational nature of faulting

The rotations of tectonic blocks about both vertical and horizontal axes are well documented in the San Felipe fault array and they help explain much of the complexity of the fault kinematics. The large hanging wall cut-off angles (~55–60°) of pre-extensional strata in the Llano El Moreno and Santa Rosa basins show that the detachment

faults initiated as steep faults and were rotated to their present orientations during progressive slip. The southern segments of both the Las Cuevitas and Santa Rosa detachments accommodate the most finite displacement and have the shallowest inclinations. In contrast, the northern segments of both of these faults become higher angle, and adjacent pre-extensional strata are less inclined. Thus, the southward-increasing displacement gradient is also associated with a southward-increasing gradient in tilting, which requires the faults and their adjacent tectonic blocks to have a 'twisted' geometry.

Lewis and Stock (1998b) and Stock et al. (1999) documented ~30–40° of clockwise vertical-axis rotation in the Sierra San Fermín and the southern Santa Rosa basin, which may help to explain the large variability in extension directions observed in the Sierra San Felipe (Fig. 12). This may be best illustrated by an exceptionally well-exposed fault surface that exhibits multiple orientations of striae (Fig. 14). The fault strikes N–S and cuts pre-extensional strata in the southern Santa Rosa basin. The rake (angle between the striae and the strike of the fault plane, measured on the fault surface) of the striae ranges from 5° to 105°, with more steeply plunging dip-slip striae systematically overprinting more shallowly plunging strike-slip striae.

There are two end-member scenarios that can explain the overprinting relationships amongst the striae observed in the fault plane shown in Fig. 14. In the first hypothesis, the fault maintains a fixed geometry and paleostress axes rotate through time. The subhorizontal extension axis rotates ~30° counter-clockwise while the shortening axis changes from horizontal to subvertical (Fig. 14b). Although this is a valid hypothesis, it does not agree with either the one-phase or two-phase kinematic models of rifting in the Gulf of California and, if representative of the regional stress field, would require a complete revision of existing kinematic models. In the second end-member hypothesis, the extension axis is held in a fixed subhorizontal E–W orientation, but the fault rotates ~30° clockwise from NW- to N-striking (Fig. 14c, d). As the angle between the fault plane and the shortening direction decreases, the fault becomes less favourably oriented for strike-slip faulting, but rotates into an ideal orientation for E–W extension and normal faulting. The ~30° clockwise rotation of the fault in this scenario agrees well with the amount of vertical axis rotation postulated for the southern Santa Rosa basin (Stock et al., 1999).

Similar clockwise rotations of fault planes might also help to explain the kinematic pattern observed in the San Felipe fault array. The wide range of orientations of extension axes in present-day fault populations of the array (Fig. 12) is very similar to the above example of the single fault surface with multiple striae (Fig. 14a, b). We propose that much of the scatter in paleostress axes in the Sierra San Felipe is due to a clockwise rotation of early-formed faults, as opposed to the rotation of paleostress axes in response to changes in the regional direction of rifting. In this case, faults with NW–SE trending extension directions should have experienced greater clockwise vertical-axis rotation than those with E–W trending extension axes. Interestingly, both end-member scenarios for the single fault plane in Fig. 14 exhibit shortening axes that define a great circle distribution, which is similar to the girdle distribution observed in the integrated fault populations of the entire fault array (Fig. 12). Local variations of the ambient stress field caused by slip on adjacent faults or fault segments are likely to have added to the observed complexity of fault-slip data.

The timing of the onset of clockwise vertical-axis rotations in the Sierra San Felipe region is critical for distinguishing between the one-phase and two-phase rifting models for the opening of the Gulf of California. Lewis and Stock (1998b) demonstrated that the ~12.6 Ma Tuff of San Felipe experienced $41 \pm 9°$ of clockwise rotation, whereas younger (~6 Ma) tuff units record $30 \pm 15°$ of clockwise rotation. They argued that the difference in clockwise rotation ($11 \pm 17°$) is statistically insignificant and therefore, they concluded that all of the clockwise rotation post-dates the ~6 Ma tuffs. This interpretation is consistent with the two-phase rifting model, in which it is believed that trans-rotational deformation within the Gulf Extensional Province did not start until ~6 Ma. We disagree with this interpretation and question the basic premise of their argument: that the Tuff of San Felipe does not record more rotation than the ~6 Ma tuffs. Even though there is some overlap in the error bars, the greater amount of clockwise rotation recorded by the Tuff of San Felipe is clearly a more robust signal than that of the ~6 Ma tuffs, meaning that while clockwise block rotations have undoubtedly affected the Sierra San Felipe since ~12.6 Ma, the exact timing of this trans-rotational deformation is not well constrained by the published paleomagnetic data. We argue that an equally valid way of interpreting their results is to conclude that ~25% of the total clockwise rotation recorded by the Tuff of San Felipe accumulated prior to ~6 Ma. This alternative interpretation should be seriously considered as it is remarkably consistent with the amount of pre-6 Ma deformation (~25%) that one would expect if strain rate was constant since the onset of deformation, which likely began at ~9–8 Ma (Seiler, 2009; also Seiler et al., in prep.). This alternative interpretation of the timing of the onset of trans-rotational deformation is also consistent with the one-phase kinematic model of rifting in the Gulf Extensional Province.

10. Transfer of onshore deformation into the Gulf of California

Much of the previous work in the Gulf Extensional Province of northern Baja California has focused on understanding the nature of strain transfer from the southern San Pedro Mártir fault onto offshore structures in the Gulf of California (Dokka and Merriam, 1982; Stock and Hodges, 1990; Nagy and Stock, 2000; Nagy, 2000; Stock, 2000). The southward decreasing displacement on the San Pedro Mártir fault, from ~5 km in the centre (Hamilton, 1971; Gastil et al., 1975) to <800 m in the south (Stock and Hodges, 1990), requires some kind of right-lateral displacement transfer, which was suggested to take place in the WNW–ESE oriented Matomí accommodation zone (Fig. 3; Stock and Hodges, 1990). Interestingly, detailed geological mapping did not reveal adequate WNW–ESE striking dextral structures in the Matomí accommodation zone (Stock and Hodges, 1990; Lewis and Stock, 1998a; Nagy, 2000; Stock, 2000), resulting in the somewhat enigmatic picture of a structural transition zone between large-displacement faults to the north, and closely spaced, small-displacement faults to the south (Stock and Hodges, 1990; Stock, 2000).

The marked displacement gradient on the San Pedro Mártir fault is in line with substantially larger displacements (up to ~9 km) on faults in the northern and central Sierra San Felipe. By contrast, fault offsets in the southern Sierra San Felipe and the Puertecitos volcanic province are typically less than 200 m and rarely exceed 500–700 m (Stock and Hodges, 1990; Lewis and Stock, 1998a; Nagy, 2000). Even though the latter are more frequent than the large-displacement faults in the north-central Sierra San Felipe, we argue that the faults in the north may have accommodated more cumulative extension, gradually decreasing towards the south. We speculate that transfer of deformation from the San Pedro Mártir fault onto Gulf of California structures occurred distributed throughout the Sierra San Felipe, rather than in a localised accommodation zone, by broad dextral shear resulting from a southward decreasing cumulative displacement and a fanning of the fault array—much in the way dextral shear was accommodated (at a different scale) in the Huatamote accommodation zone.

This scenario invariably produces vertical-axis rotations in the hanging wall of the listric San Pedro Mártir fault, probably above a basal detachment, which is consistent with the clockwise vertical-axis rotations reported for the Sierras San Felipe and San Fermín (Lewis and Stock, 1998b; Stock et al., 1999). However, it does not necessitate the existence of hidden structures accommodating additional strike-slip in the Matomí accommodation zone (Fig. 3), nor a WNW–ESE striking transition zone separating clockwise rotations to the north (Lewis and

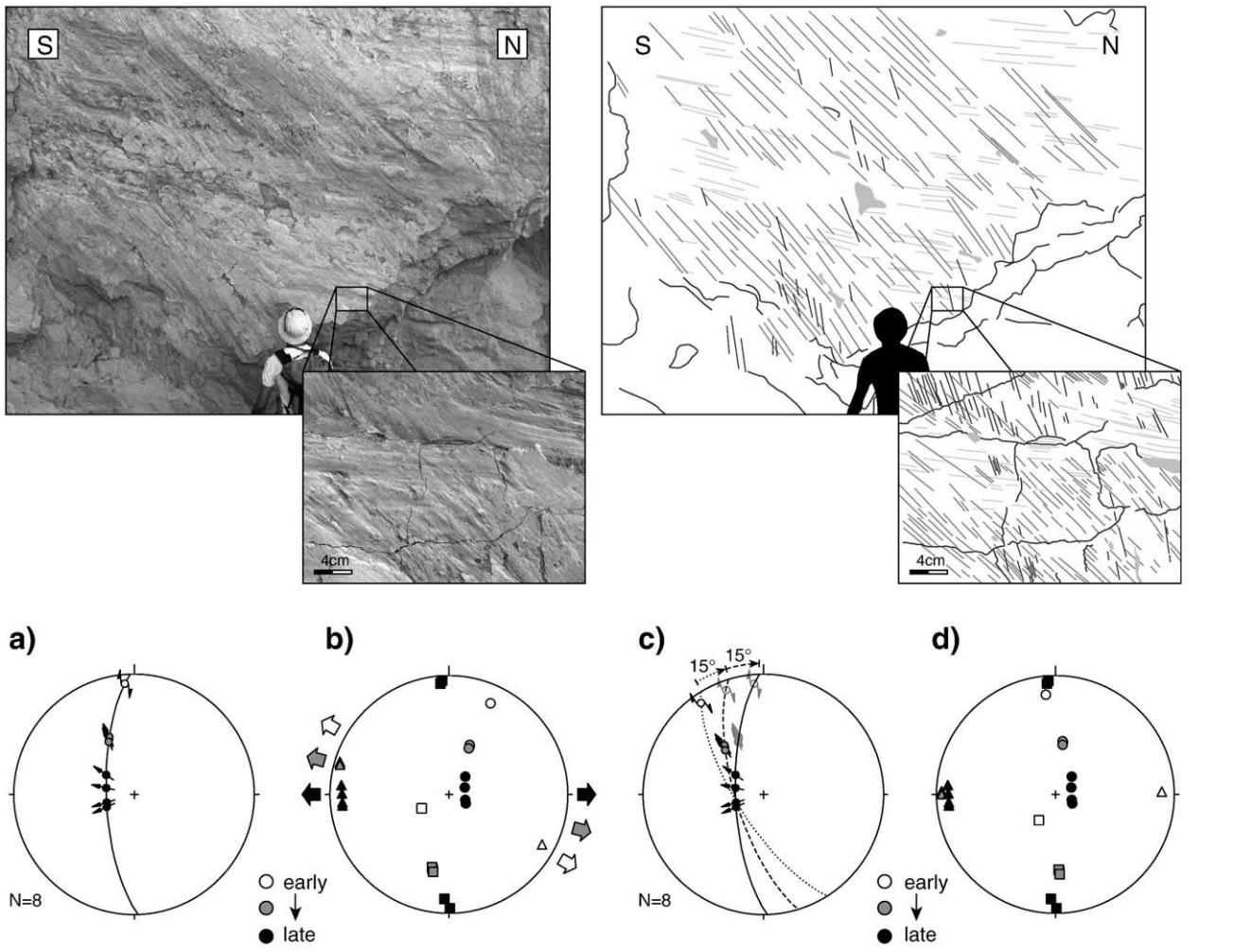

Fig. 14. Photo and sketch of a currently N–S striking fault plane that shows shallow slickenlines with dextral shear sense being progressively overprinted by oblique-, then dip-slip striae. The fault cuts Paleogene to earliest Miocene sediments and may thus have formed at any time during Neogene rifting. Stereoplots show the current configuration of the fault plane (a) and two alternative interpretations: (b) fixed fault plane and counter-clockwise rotation of the stress field; or (c, d) clockwise rotation of the fault plane within a stationary transtensional stress regime and E–W extension. Progressive clockwise rotation may have turned the fault into parallelism with the N–S compression direction, causing a permutation of the shortening and intermediate axes leading to its reactivation as a normal fault. Paleostress orientations are shown with compression directions as circles, intermediate axes as squares, and extension directions (trend) marked by triangles (arrows).

Stock, 1998b; Stock et al., 1999) from <10° in the south (Nagy, 2000). Instead, vertical-axis rotations in the Sierra San Felipe would increase with distance from the Main Gulf Escarpment in a west towards east rather than south towards north direction, with maximum clockwise rotations of ~30–40° in the Sierra San Fermín (Lewis and Stock, 1998b). Unfortunately, existing paleomagnetic data north of the inferred Matomí accommodation zone have been collected in comparable structural positions to the east of the Las Cuevitas, Santa Rosa and Huatamote detachments, arguably the most important exposed structures in the hanging wall of the San Pedro Mártir fault. Further studies, particularly from the footwall of these three detachments, are necessary to test the above model of broad right-lateral displacement distributed throughout the Sierra San Felipe.

11. Conclusions

Neogene rifting in the Sierra San Felipe was dominated by integrated normal and strike-slip faulting on three major detachment faults that control the eastern margins of the Sierras San Felipe and Santa Rosa. The faults are arranged in a left-stepping en-echelon configuration and are linked by accommodation and transfer zones. The Santa Rosa and Las Cuevitas detachments each accommodated a major southward-increasing displacement gradient with up to ~7.5–9 km of broadly E- to SE-directed displacement, and their inclination varies systematically from high and moderate angles in the north to shallow angles in the south.

Stratigraphic relationships in three major rift basins in the hanging wall of the detachments demonstrate that extension started after deposition of the Tuff of San Felipe (~12.6 Ma) and an andesite flow that locally overlies it. Slip rates on the detachments peaked in the latest Miocene to Pliocene time when sedimentation was dominated by lacustrine and marine strata in the Santa Rosa and Llano El Moreno basins, respectively. The faults are overlapped by Pleistocene alluvial fan deposits, which represent the time when slip on the detachments ceased.

Fault striations show no systematic overprinting between dominant NNW- to NE-striking normal faults, and conjugate NNW-striking dextral and ENE-striking sinistral faults. Instead, the kinematic behaviour of faults reflects the spatial orientation of fault planes with respect to the fixed orientation of a protracted transtensional stress regime. Paleostress reconstructions derived from fault-plane solutions of fault-slip data yield bulk extension directions ranging from NE to SE, and compression axes that permutate between subvertical and subhorizontal for the late Miocene to present stress regime. Most of the kinematic complexity indicated by analysis of fault striae can best be explained by clockwise vertical-axes rotations

that we infer to have accompanied the entire history of slip on the detachments.

In addition to vertical thinning and horizontal extension of the crust, the San Felipe fault array accommodated a significant component of N–S horizontal shortening, which is well documented by the distribution of paleostress axes of the integrated fault populations, E–W striking reverse faults and E–W trending constrictional folds. Megamullion deflections on the detachments are also attributed constrictional folding, which started at the earliest stages of rifting. This overall constrictional strain regime is indistinguishable from the modern strain regime in the Gulf Extensional Province, and we interpret the San Felipe fault array to have formed during a single phase of integrated transtensional shearing from the time of its inception in the late Miocene.

Acknowledgements

This research was partially funded by ARC DP0665127 to AJWG and BPK, and by grants CONACYT #81463 grants to and NSF EAR-0739017 Sub-Award 08-004375-01 JMF. Additional support was provided to CS by MIFRS, MIRS and MATS scholarships from the University of Melbourne and the David Hay Memorial Fund. The author is especially grateful to Yvonne Kunz for invaluable support and assistance in the field. Ramón Mendoza-Borunda, Arturo Martín-Barajas and the staff at CICESE are thanked for their help and logistical support. Chris Wilson provided the software used for fault-slip analysis. David Foster and Jon Spencer made valuable comments on an early version of this manuscript. We thank two anonymous reviewers for thoughtful and constructive reviews which greatly helped to improve the quality of the manuscript, and Ibrahim Çemen for the editorial handling of the manuscript.

References

Allen, C.R., Silver, L.T., Stehli, F.G., 1960. Agua Blanca fault — a major transverse structure of northern Baja California, Mexico. Geological Society of America Bulletin 71 (4), 457–482.

Andersen, R.L., 1973. Geology of the Playa San Felipe Quadrangle, Baja California, Mexico. MSc thesis, California State University San Diego.

Angelier, J., Colletta, B., Chorowicz, J., Ortlieb, L., Rangin, C., 1981. Fault tectonics of the Baja California Peninsula and the opening of the Sea of Cortez, Mexico. Journal of Structural Geology 3 (4), 347–357.

Axen, G.J., Fletcher, J.M., 1998. Late Miocene–Pleistocene extensional faulting, northern Gulf of California, Mexico and Salton Trough, California. International Geology Review 40 (3), 217–244.

Bingham, C., 1964. Distributions on the sphere and on the projective plane. PhD thesis, Yale University.

Black, N., 2004. Structure and hanging wall stratigraphy of the Las Cuevitas detachment, central Sierra San Felipe, Baja California, Mexico. MSc thesis, University of California Los Angeles.

Boehm, M.C., 1984. An overview of the lithostratigraphy, biostratigraphy, and paleoenvironments of the late Neogene San Felipe marine sequence, Baja California Sur, Mexico. Field Trip Guidebook — Pacific Section: Society of Economic Paleontologists and Mineralogists, vol. 39, pp. 253–265.

Brown, L.G., 1978. Recent fault scarps along the eastern escarpments of the Sierra San Pedro Mártir, Baja California. MSc thesis, San Diego State University.

Bryant, B.A., 1986. Geology of the Sierra Santa Rosa basin, Baja California, Mexico. MSc thesis, San Diego State University.

DeMets, C., 1995. A reappraisal of seafloor spreading lineations in the Gulf of California: implications for the transfer of Baja California to the Pacific Plate and estimates of Pacific–North America motion. Geophysical Research Letters 22 (24), 3545–3548.

DeMets, C., Dixon, T.H., 1999. New kinematic models for Pacific–North America motion from 3 Ma to present, I: evidence for steady motion and biases in the NUVEL-1A model. Geophysical Research Letters 26 (13), 1921–1924.

Dixon, T.H., Fletcher, J.M., Marquez-Azua, B., Miller, M., Sanchez, O., Umhoefer, P., Farina, F., DeMets, C., Suarez-Vidal, F., 2000. New kinematic models for Pacific–North America motion from 3 Ma to present, II: evidence for a "Baja California shear zone". Geophysical Research Letters 27 (23), 3961–3964.

Dixon, T.H., Decaix, J., Farina, F., Furlong, K., Malservisi, R., Bennett, R., Suarez-Vidal, F., Fletcher, J.M., Lee, J., 2002. Seismic cycle and rheological effects on estimation of present-day slip rates for the Agua Blanca and San Miguel–Valecitos faults, northern Baja California, Mexico. Journal of Geophysical Research 107 (B10), 2226.

Dokka, R.K., Merriam, R.H., 1982. Late Cenozoic extension of northeastern Baja California, Mexico. Geological Society of America Bulletin 93 (5), 371–378.

Dorsey, R.J., Burns, B., 1994. Regional stratigraphy, sedimentology, and tectonic significance of Oligocene–Miocene sedimentary and volcanic rocks, northern Baja–California, Mexico. Sedimentary Geology 88 (3–4), 231–251.

Esser, R.P., McIntosh, W.C., 2003. $^{40}Ar/^{39}Ar$ Geochronology Results from the Bay of Los Angeles, Baja, Mexico. Open File Report OF-AR-19, New Mexico Bureau of Geology and Mineral Resources.

Faulds, J.E., Varga, R.J., 1998. The Role of Accommodation Zones and Transfer Zones in the Regional Segmentation of Extended Terranes. In: Faulds, J.E., Stewart, J.H. (Eds.), Accommodation Zones and Transfer Zones: The Regional Segmentation of the Basin and Range Province: Geological Society of America Special Paper, vol. 323, pp. 1–45.

Faulds, J.E., Olson, E.L., Harlan, S.S., McIntosh, W.C., 2002. Miocene extension and fault-related folding in the Highland Range, southern Nevada: a three-dimensional perspective. Journal of Structural Geology 24 (4), 861–886.

Fenby, S.S., Gastil, R.G., 1991. Geologic-tectonic map of the Gulf of California and surrounding areas. American Association of Petroleum Geologists Memoir 47, 79–83.

Fletcher, J.M., Bartley, J.M., 1994. Constrictional strain in a non-coaxial shear zone: implications for fold and rock fabric development, central Mojave metamorphic core complex, California. Journal of Structural Geology 16 (4), 555–570.

Fletcher, J.M., Mungúia, L., 2000. Active continental rifting in southern Baja California, Mexico: implications for plate motion partitioning and the transition to seafloor spreading in the Gulf of California. Tectonics 19 (6), 1107–1123.

Fletcher, J.M., Bartley, J.M., Martin, M.W., Glazner, A.F., Walker, J.D., 1995. Large-magnitude continental extension: an example from the central Mojave metamorphic core complex. Geological Society of America Bulletin 107 (12), 1468–1483.

Fletcher, J.M., Grove, M., Kimbrough, D., Lovera, O., Gehrels, G.E., 2007. Ridge–trench interactions and the Neogene tectonic evolution of the Magdalena Shelf and southern Gulf of California: insights from detrital zircon U–Pb ages from the Magdalena Fan and adjacent areas. Geological Society of America Bulletin 119 (11–12), 1313–1336.

Gastil, R.G., Phillips, R.P., Allison, E.C., 1975. Reconnaissance geology of the State of Baja California. Geological Society of America Memoir 140, 170p.

Hamilton, W.B., 1971. Recognition on Space Photographs of Structural Elements of Baja California. U. S. Geological Survey Professional Paper 718, U. S. Geological Survey.

Harvey, T.W., 1985. Geology of the San Miguel fault zone, northern Baja California, Mexico. MSc thesis, San Diego State University.

Hausback, B.P., 1984. Cenozoic volcanic and tectonic evolution of Baja California Sur, Mexico. Field Trip Guidebook — Pacific Section: Society of Economic Paleontologists and Mineralogists, vol. 39, pp. 219–236.

Hilinski, T.E., 1988. Structure and Quaternary faulting about the eastern terminus of the Agua Blanca Fault, Baja California, Mexico. MSc thesis, San Diego State University.

Hirabayashi, C.K., Rockwell, T.K., Wesnousky, S.G., Stirling, M.W., Suarez-Vidal, F., 1996. A neotectonic study of the San Miguel-Vallecitos Fault, Baja California, Mexico. Bulletin of the Seismological Society of America 86 (6), 1770–1783.

Janecke, S.U., Vandenburg, C.J., Blankenau, J.J., 1998. Geometry, mechanisms and significance of extensional folds from examples in the Rocky Mountain Basin and Range province. U.S.A. Journal of Structural Geology 20 (7), 841–856.

John, B.E., 1987. Geometry and Evolution of a Mid-crustal Extensional Fault System: Chemehuevi Mountains, Southeastern California. In: Coward, M.P., Dewey, J.F., Hancock, P.L. (Eds.), Continental Extensional Tectonics: Geological Society of London Special Publications, vol. 28, pp. 313–335.

Karig, D.E., Jensky, W., 1972. The proto-Gulf of California. Earth and Planetary Science Letters 17 (1), 169–174.

Lee, J., Miller, M.M., Crippen, R., Hacker, B., Vazquez, J.L., 1996. Middle Miocene extension in the Gulf Extensional Province, Baja California: evidence from the southern Sierra Juarez. Geological Society of America Bulletin 108 (5), 505–525.

Lewis, C.J., 1994. Constraints on extension in the Gulf Extensional Province from the Sierra San Fermín, northeastern Baja California, Mexico. PhD thesis, Harvard University.

Lewis, C.J., Stock, J.M., 1998a. Late Miocene to Recent transtensional tectonics in the Sierra San Fermín, northeastern Baja California, Mexico. Journal of Structural Geology 20 (8), 1043–1063.

Lewis, C.J., Stock, J.M., 1998b. Paleomagnetic evidence of localized vertical axis rotation during Neogene extension, Sierra San Fermín, northeastern Baja California, Mexico. Journal of Geophysical Research 103 (B2), 2455–2470.

Lonsdale, P.F., 1989. Geology and Tectonic History of the Gulf of California. In: Winterer, E.L., Hussong, D.M., Decker, R.W. (Eds.), The Geology of North America: The Eastern Pacific Ocean and Hawaii, pp. 499–521.

Lonsdale, P.F., 1991. Structural patterns of the Pacific floor offshore of Peninsular California. American Association of Petroleum Geologists Memoir 47, 87–125.

Mancktelow, N.S., Pavlis, T.L., 1994. Fold-fault relationships in low-angle detachment systems. Tectonics 13 (3), 668–685.

Michaud, F., Sosson, M., Royer, J.Y., Chabert, A., Bourgois, J., Calmus, T., Mortera, C., Bigot-Cormier, F., Bandy, W., Dyment, J., Pontoise, B., Sichler, B., 2004. Motion partitioning between the Pacific Plate, Baja California and the North America Plate: The Tosco–Abreojos Fault revisited. Geophysical Research Letters 31 (8), 4.

Nagy, E.A., 2000. Extensional deformation and paleomagnetism at the western margin of the Gulf extensional province, Puertecitos Volcanic Province, norteastern Baja California, Mexico. Geological Society of America Bulletin 112 (6), 857–870.

Nagy, E.A., Stock, J.M., 2000. Structural controls on the continent–ocean transition in the northern Gulf of California. Journal of Geophysical Research 105 (B7), 16251–16269.

Nagy, E.A., Grove, M., Stock, J.M., 1999. Age and stratigraphic relationships of pre- and syn-rift volcanic deposits in the northern Puertecitos volcanic province, Baja California, Mexico. Journal of Volcanology and Geothermal Research 93 (1–2), 1–30.

Ness, G.E., Lyle, M.W., 1991. A seismo-tectonic map of the Gulf and Peninsular Province of the Californias. American Association of Petroleum Geologists Memoir 47, 71–77.
Oskin, M., 2002. Part I. Tectonic evolution of the northern Gulf of California, Mexico, deduced from conjugate rifted margins of the upper Delfín Basin; Part II. Active folding and seismic hazard in central Los Angeles, California. PhD thesis, California Institute of Technology.
Oskin, M., Stock, J.M., 2003a. Cenozoic Volcanism and Tectonics of the Continental Margins of the Upper Delfín Basin, Northeastern Baja California and Western Sonora. In: Johnson, S.E., Paterson, S.R., Fletcher, J.M., Girty, G.H., Kimbrough, D.L., Martín-Barajas, A. (Eds.), Tectonic Evolution of Northwestern México and the Southwestern USA: Geological Society of America Special Paper, vol. 374, pp. 421–438.
Oskin, M., Stock, J.M., 2003b. Pacific–North America plate motion and opening of the Upper Delfín basin, northern Gulf of California, Mexico. Geological Society of America Bulletin 115 (10), 1173–1190.
Petit, J.P., 1987. Criteria for the sense of movement on fault surfaces in brittle rocks. Journal of Structural Geology 9 (5–6), 597–608.
Schlische, R.W., 1995. Geometry and origin of fault-related folds in extensional settings. American Association of Petroleum Geologists Bulletin 79 (11), 1661–1678.
Seiler, C., 2009. Structural and thermal evolution of the Gulf Extensional Province in Baja California, Mexico: Implications for Neogene rifting and opening of the Gulf of California. PhD thesis, The University of Melbourne.
Seiler, C., Fletcher, J.M., Kohn, B.P., Gleadow, A.J.W., Raza, A., in prep. Low-temperature thermochronology of the San Felipe detachment system: Significance of decoupled slip-exhumation gradients in transtensional strain and the timing of rifting in the northern Gulf of California. In preparation for Tectonics.
Spencer, J.E., 1984. Role of tectonic denudation in warping and uplift of low-angle normal faults. Geology 12 (2), 95–98.
Spencer, J.E., 1999. Geologic continuous casting below continental and deep-sea detachment faults and at the striated extrusion of Sacsayhuaman, Peru. Geology 27 (4), 327–330.
Spencer, J.E., 2000. Possible origin and significance of extension-parallel drainages in Arizona's metamorphic core complexes. Geological Society of America Bulletin 112 (5), 727–735.
Spencer, J.E., Normark, W.R., 1979. Tosco–Abreojos fault zone: a Neogene transform plate boundary within the Pacific margin of southern Baja California, Mexico. Geology 7 (11), 554–557.
Stock, J.M., 1993. Geologic map of southern Valle Chico and adjacent regions, Baja California, Mexico. Geological Society of America — Map and Chart Series MCH076.
Stock, J.M., 2000. Relation of the Puertecitos Volcanic Province, Baja California, Mexico, to Development of the Plate Boundary in the Gulf of California. In: Delgado-Granados, H., Aguirre-Díaz, G., Stock, J.M. (Eds.), Cenozoic Tectonics and Volcanism of Mexico: Geological Society of America Special Paper, vol. 334, pp. 143–156.
Stock, J.M., Hodges, K.V., 1989. Pre-Pliocene extension around the Gulf of California and the transfer of Baja California to the Pacific plate. Tectonics 8 (1), 99–115.
Stock, J.M., Hodges, K.V., 1990. Miocene to Recent structural development of an extensional accommodation zone, northeastern Baja California, Mexico. Journal of Structural Geology 12 (3), 315–328.
Stock, J.M., Lewis, C.J., Nagy, E.A., 1999. The Tuff of San Felipe: an extensive middle Miocene pyroclastic flow deposit in Baja California, Mexico. Journal of Volcanology and Geothermal Research 93 (1–2), 53–74.
Umhoefer, P.J., Mayer, L., Dorsey, R.J., 2002. Evolution of the margin of the Gulf of California near Loreto, Baja California Peninsula, Mexico. Geological Society of America Bulletin 114 (7), 849–868.
Wallbrecher, E., 1986. Tektonische und gefügeanalytische Arbeitsweisen: Graphische, rechnerische und statistische Verfahren. Ferdinand Enke Verlag, Stuttgart.
Wetmore, P.H., Schmidt, K.L., Paterson, S.R., Herzig, C., 2002. Tectonic implications for the along-strike variation of the Peninsular Ranges batholith, southern and Baja California. Geology 30 (3), 247–250.
Wetmore, P.H., Herzig, C., Alsleben, H., Sutherland, M., Schmidt, K.L., Schultz, P.W., Paterson, S.R., 2003. Mesozoic Tectonic Evolution of the Peninsular Ranges of Southern and Baja California. In: Johnson, S.E., Paterson, S.R., Fletcher, J.M., Girty, G.H., Kimbrough, D.L., Martín-Barajas, A. (Eds.), Tectonic Evolution of Northwestern México and the Southwestern USA: Geological Society of America Special Paper, vol. 374, pp. 93–116.
Yin, A., Dunn, J.F., 1992. Structural and stratigraphic development of the Whipple–Chemehuevi detachment fault system, southeastern California: implications for the geometrical evolution of domal and basinal low-angle normal faults. Geological Society of America Bulletin 104 (6), 659–674.
Zanchi, A., 1994. The opening of the Gulf of California near Loreto, Baja California, Mexico: from basin and range extension to transtensional tectonics. Journal of Structural Geology 16 (12), 1619–1639.